Universiteit Utrecht

University of California, Berkeley

Rapid Design and Evaluation of Swing-Type Check Valves

Bachelor's Thesis

Author:
Joost De Jong

Supervisors:
Prof. dr. Rene van Roij
Prof. M. Reza Alam
Marcus Lehmann, M.Sc.

June 17, 2014

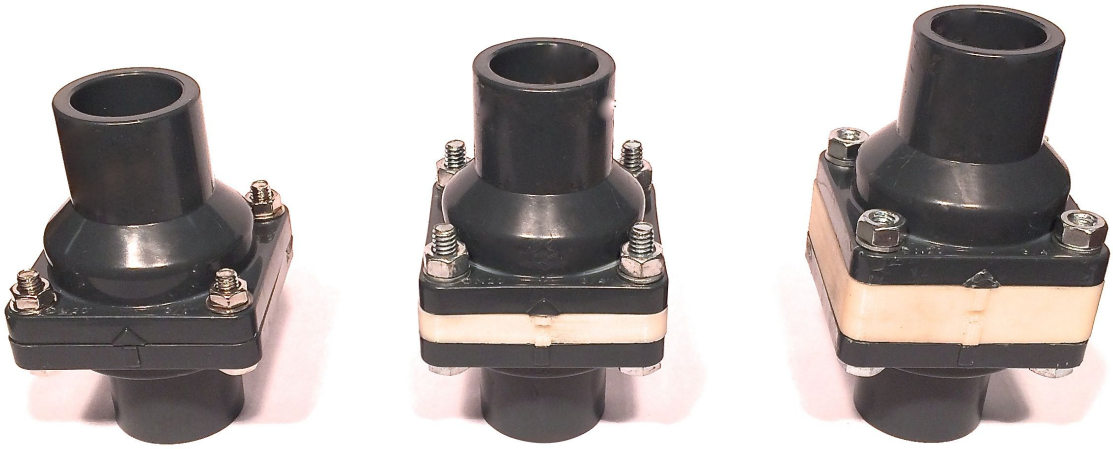

Abstract

The Theoretical and Applied Fluid Dynamics Laboratory (*TAFLab*) at the University of California, Berkeley is investigating several designs for novel shallow water wave energy converters. The common denominator for these prototypes is that they operate with a hydraulic power takeoff (*PTO*) for the secondary power conversion. A critical component of an hydraulic PTO is one or more check valves creating a unidirectional flow. The research goal of this thesis is the flow optimization of these components. Turbulence in the check valves was assumed to be a major cause for efficiency losses in the current PTO design.

Computer Aided Design (*CAD*) and rapid prototyping through Fused Deposition Modeling (*FDM*) were selected as prototyping tools, due to the high customizability and short lead time of components. Experimental analysis and fluid simulations were used to compare and verify the performance of the optimized check valve designs.

One of the performance measures for check valves is the head loss coefficient K_v, which is desired to be low in the flow direction, and high in the reverse direction. We observed that the original check valve had a $K_{v,D} = 57.2 \pm 1.0$ in the flow direction and no flow in the reverse direction ($K_{v,R} = \infty$). A minor modification improved $K_{v,D}$ to 46.1 ± 0.9 in the flow direction but 'decreased' $K_{v,R} = 8.7 \pm 1.7 \cdot 10^7$ in the reverse direction. The first double door design brought $K_{v,D}$ down to 6.4 ± 0.5, but with a reverse loss coefficient of 738 ± 11. The final double door check valve had a $K_{v,D}$ of 8.4 ± 0.5 in the flow direction and $K_{v,R} = 1.4 \pm 0.3 \cdot 10^6$ in the reverse direction, and was selected for a dynamic test.

In a direct application in a pumping setup, we however observed an efficiency decrease from $41.3 \pm 0.5\%$ to $24.7 \pm 0.5\%$, possibly explained by the closing speeds of the new valve. It is concluded that optimizing losses in a steady state flow experiment cannot guarantee improved results in pulsating or alternating flow.

Contents

1 Introduction

The Theoretical and Applied Fluid Dynamics Laboratory (*TAFLab*, [1]) at the University of California, Berkeley is investigating several designs for novel shallow water wave energy converters. At present, inspired by the energy absorbing capabilities of a muddy seafloor, working prototypes of a so-called 'wave carpet' have been developed, designed to efficiently pump water through the mechanical motion of a silicone sheet [2] [3]. Current investigations include the optimal damping factors, positions of the pumps and carpet stiffness optimization. See Fig. 1 for one of the prototypes in the lab wavetank.

Originally focused on a newly developed alternative design, the goal of this thesis is to further the research in harvesting wave energy by investigation of the current check valves, a critical component in regulating the flow. It was conceived that the alternative prototype struggled because of major pressure losses in its valves, and there were indications that the efficiency of the wave carpet could be improved as well. A reduction in pressure losses by optimizing the design of the check valves will leave more pressure for the system outlets, and consequent energy generation or, as originally suggested, a desalination process using reverse osmosis.

This work starts with an introduction into the hydraulics of pipelines (Sec. 2, and the equations necessary to develop an experiment to measure a component's head losses in a steady state flow. The experimental setup is discussed (Sec. 3), and foreshadowing to the experimental results (Sec. 5), design choices are motivated (Sec. 4). Finally, the conclusion is drawn (Sec. 6) and this and future work is discussed (Sec 7).

A trade-off decision between costs, performance and lead time was made by developing a new component that was easily integrable with existing hardware, and quick to create. Computer Aided Design (*CAD*) and rapid prototyping through Fused Deposition Modeling (*FDM*) were selected as prototyping tools, due to the high customizability (and therefore hardware integration) and short lead time of components (many designs can be tested).

Hereby I would like to thank the members of the *TAFLab* and the Education Abroad Program (*EAP*) for providing me with the opportunity to conduct my undergraduate thesis research abroad at the world's number one public institution. It has ignited my interest in pursuing an engineering degree in the years to come.

Figure 1: The Wave Carpet in action in the O'Brien wave tank

2 Theory

2.1 Hydraulics of Pipelines

The literature on flow though pipes and valves has evolved to a practical engineering approach. More than trying to understand flow characteristics and the interaction of various components in a system, the focus is mainly on quick calculating methods and the literature is filled with empirical tables.

The analysis of piping systems is generally through a one-dimensional approach [4]. By Bernoulli's Principle, the change in static head between two points equals

$$z_1 + h_1 + \frac{\bar{u}_1^2}{2g} = z_2 + h_2 + \frac{\bar{u}_2^2}{2g} + h_L \tag{1}$$

where $\bar{u}$ is the mean velocity, $\frac{\bar{u}^2}{2g}$ is the velocity head (see. Fig 2), g the gravitational acceleration, z is the elevation above a fixed datum, h is the static head and h_L is the head loss between two stations (eg. 1 and 2). The velocity head and the static head combined equal the total head of the system at a certain location. Observe that in a linear piping system with equal inlet and outlet diameter, no velocity head is lost, since the mean flow velocity remains constant ($\bar{u}_1 = \bar{u}_2$).

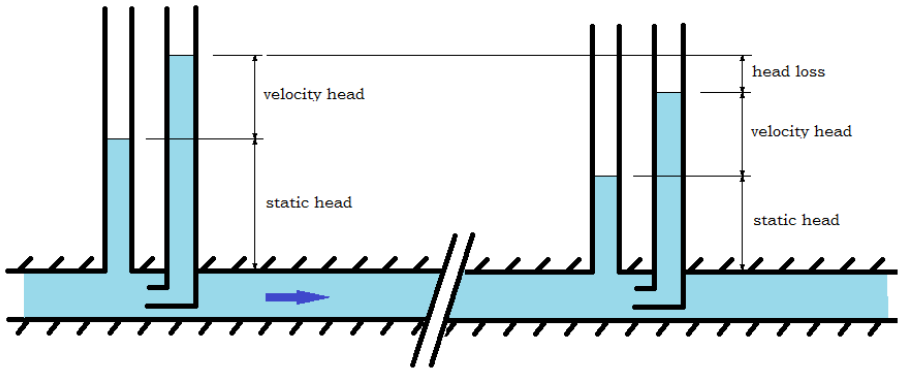

Figure 2: Head loss in a linear piping system

It is found that component head losses approximately scale with the square of the flow velocity. Therefore, it makes sense to define a non-dimensional head loss coefficient K of the ratio of the head loss by the velocity head (see Eq. 2) K is an important numeric for the treatment of losses in pipes, bends, valves and various other components in a one-dimensional model.

$$K = \frac{2gh_L}{\bar{u}_i^2} \tag{2}$$

Given the flow velocities $\bar{u}_i$ and head loss coefficients K_i of components of a linear system, the total head loss between the in- and outlet simply equals

$$h_L = \sum K_i \frac{\bar{u}_i^2}{2g} \tag{3}$$

2.1.1 Pipe loss coefficients

For a scalable component such as a pipe, the head loss has been analytically determined and is given by the Darcy-Weisbach equation, written in classical form as

$$h_L = f\frac{L}{D}\frac{\bar{u}^2}{2g} \tag{4}$$

where $\frac{L}{D}$ is the length to diameter ratio of the pipe, and f is the dimensionless Darcy friction factor. Equation 4 leads to a pipe loss coefficient K_p of

$$K_p = f\frac{L}{D} \tag{5}$$

For the laminar flow regime, the Darcy friction factor was analytically determined by Poiseuille. This can be done by equating the Darcy-Weisbach equation with the Hagen-Poiseuille equation for pressure drop:

$$\Delta p = f\frac{L}{D}\rho\frac{\bar{u}^2}{2} = \frac{128\mu QL}{\pi D^4} \tag{6}$$

$$f = \frac{256Q\mu}{D^3\pi\bar{u}^2\rho} = \frac{64\mu}{D\bar{u}\rho} = \frac{64}{R_e} \tag{7}$$

where ρ is the fluid density, μ is the fluid dynamic viscosity, and Q is the volumetric flow rate. However, for more turbulent flows, the factor also becomes dependent on the relative roughness of the piping material. There are various (empirical) resources such as the Moody Table (see Fig. 3) or formulae available relating these influences to the friction factor, one of which being the Colebrook-White formula [5]:

$$\frac{1}{\sqrt{f}} = -2\log_{10}\left(\frac{2.51}{R_e\sqrt{f}} + \frac{k}{3.7D}\right) \tag{8}$$

where k is the absolute roughness height and D the pipe diameter. The ratio $\frac{k}{D}$ is often referred to as the relative roughness factor. A solution to this implicit equation in f can be obtained by iterative methods, or by one of various explicit approximations [6].

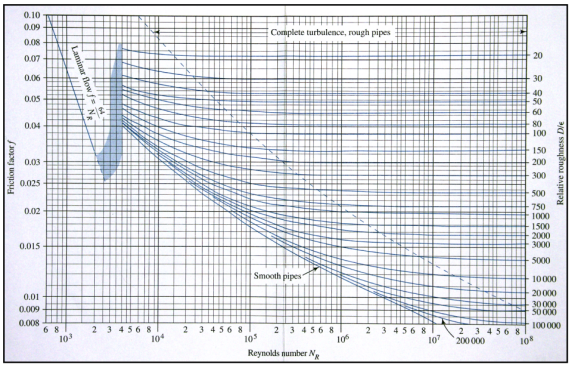

Figure 3: A lookup table for the Darcy Factor

2.1.2 Bend loss coefficients

For pipe bends, an array of tables for the head loss coefficient is available. Given the radius to diameter ratio $\frac{r}{D}$ and the turning angle θ, Figure 4 gives $K_{b,10^6}$ for smooth circular bends at a Reynolds number of 10^6, with relatively long pipes connected to the in- and outlet of the bend ($\frac{L}{D} > 30$). These values have been determined mostly empirically, in setups where the bend is an isolated component. The relative long in- and outlet tangents are needed to let the flow redevelop after flowing through the bend, therefore fully including the downstream effects to the head loss.

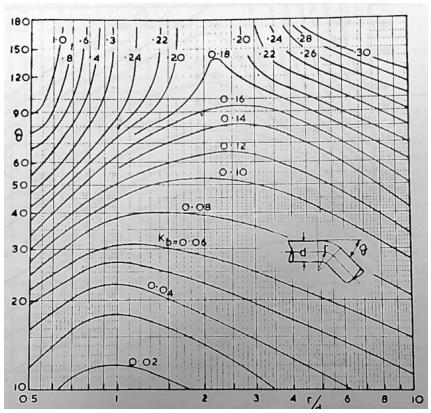

Figure 4: A lookup table for the bend loss coefficient in smooth circular pipes

For flow at other Reynolds numbers, or for a bend with relatively short outlet tangents, correction factors are available, such that the actual loss coefficient is given by

$$K_b = \alpha_{R_e} \beta_b K_{b,10^6} \tag{9}$$

where α_{R_e} is the Reynolds number correction coefficient and β_b is the outlet tangent correction coefficient (See Fig. 6).

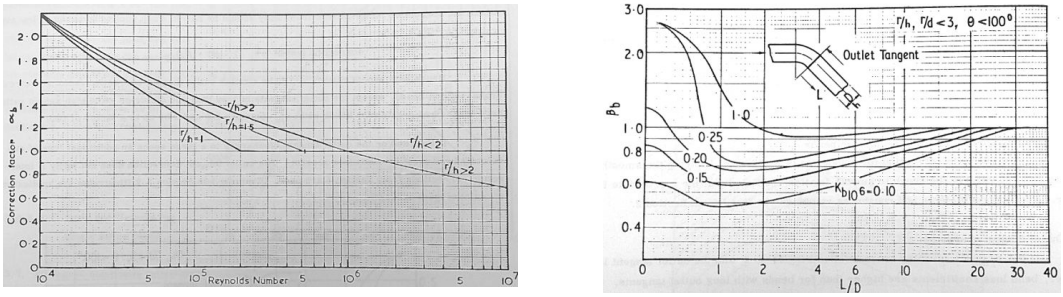

Figure 6: Correction factors for other Reynolds numbers (left) or outlet tangents (right)

2.1.3 Valve loss coefficients

In addition to being proportional to the square of the flow velocity, the head loss across a valve is also dependent on the valve opening. Manufacturers' approximations can only give rough estimations of valve loss coefficients for a number of reasons, therefore requiring our experimental investigation. Miller [4] states:

- Loss coefficients are often based on the pressure differential between points immediately before and just after the valves. As the influence of the valve extends thirty or more diameters downstream, the percentage error in the loss coefficients of low loss valves (say $K_v < 0.5$) is often high;
- Usually geometric similarity does not exist either between valve sizes or between valves from different manufacturers;
- Normally only nominal dimensions and not actual dimensions are given (loss coefficients vary as the fourth power of the error);
- Reynolds number effects are often neglected.

Tullis [7] specifies the approximate valve losses only for the manual valves (see Fig. 7), by the so-called discharge coefficient C_d:

$$K_v = \frac{1}{C_d^2} - 1 \tag{10}$$

$$C_d = \frac{\bar{u}}{\sqrt{2gh_L + \bar{u}^2}} = \frac{1}{\sqrt{K_v + 1}} \tag{11}$$

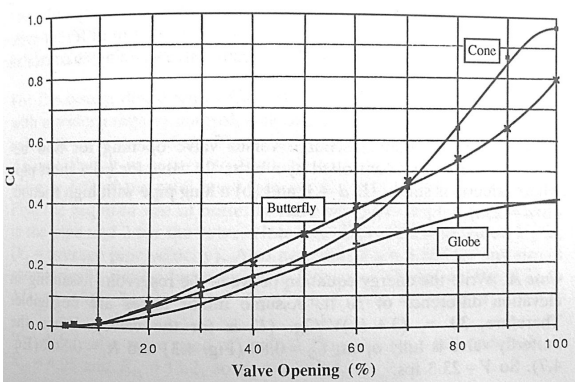

Figure 7: Discharge coefficients for butterfly, cone and globe manual valves

It can be seen that an open cone valve has a discharge coefficient close to one, equivalent to a near-zero valve head loss coefficient K_v.

For comparison with the literature, a number of predictions for the relevant design types of check valves (assumed fully open) is given in Fig. 8.

			Miller	Tullis	Jianhua
Design	Cone	Original	0.1	0.08	
	Hinged	Original	1		5.8*
		Widened	1		1*
	Double door	Non-Sealed	0.3	0.56	
		Sealed	0.3	0.56	

Figure 8: Table of predicted valve loss coefficients K_v

Although there is clearly some variability, qualitatively, we can expect a small losses in the cone valve ($K_v << 1$), and a better performance in steady state flow of the double door valve versus the hinged valve. In pulsating flow, such as in the piston pumps used in the wave carpet, other characteristics may need to be taken into account, such as closing speeds or sealing capabilities. Sealing capabilities are quantitatively tested by observing the flow through the check valve in a reversed position, but none of the cited sources quantified these characteristics.

2.1.4 Orifice Plate loss coefficients

In the original hinge valve design, two orifice restrictions are visible in the cross-section of the valve (see Design Section 4.1.1 and Appendix B.1). Although most orifice loss coefficients are based on a standalone component, such as in the experiment by Jianhua [8], an indication of the influence of removing these orifices from the valve design was desired.

Their result was an experimental fit, valid for diameter ratios $0.4 \leq \beta \leq 0.8$, and ratios of pipe diameter and orifice thickness $0.05 \leq \alpha \leq 0.25$ for a flow with $R_e > 10^5$:

$$K_{or} = \frac{0.7418}{\alpha^{0.1142}} \left(\frac{3.196}{\beta^4} - \frac{5.646}{\beta^2} + 2.45 \right) \tag{12}$$

Assuming the hinge valve with removed orifices has a head loss coefficient of 1 (as by Miller), the original hinge valve losses are estimated by

$$K_v^* = K_v + 2K_{or} = K_v + 2 \cdot 2.4 = 5.8 \tag{13}$$

*A numeric for the effect of removing the orifices inside the original hinge valve was desired. The widened valve was assumed to have loss coefficient 1 (as by Miller) and the added losses were calculated in Sec. 2.1.4

2.1.5 Inlets and Outlet loss coefficients

The pipe inlet at the constant head tank and the pipe outlet at the exit tank induce some losses due to the developing flow after the contraction/expansion. An exit can be treated as the limit of an abrupt expansion in pipe diameter [9], where the second diameter approaches infinity:

$$K_{exit} = \lim_{D_2 \to \infty} \left(1 - \left(\frac{D_1}{D_2}\right)^2\right)^2 = 1 \tag{14}$$

For the inlet however, no analytic expression can be derived, and various sources (Miller, Benedict) approximate the losses by using $K_{in} = 0.5$ (See Fig. 9

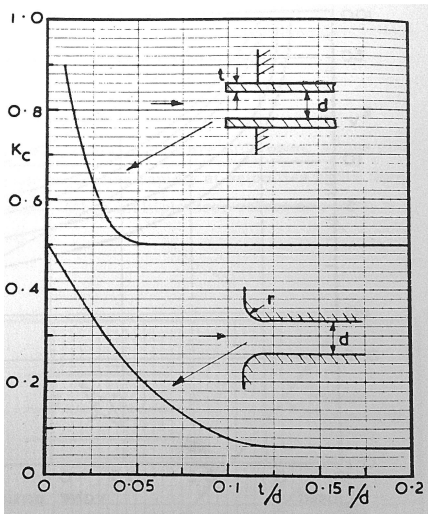

Figure 9: Empirical loss coefficients for flush and re-entrant inlets

2.2 Middle-Value Theorem for calculations with a finite exit tank

Should the exit of the piping system be a finite tank with rising water level as time progresses, filled by the flow through the check valve, then the average flow speed can not be calculated directly. The rising water level namely influences the difference in water height through the piping system, in turn decreasing the flow as the exit tank fills.

Assuming the average flow speed $\bar{u}$ and exit tank water level y can be measured and the filling characteristics (liters per centimeter) are known, an analytic solution is still possible. Say $V_{exit}(y)$ is the total volume of water contained in the exit tank as a function of water height y. Then by the mean value theorem, during the filling of the tank, there is a height y^* such that the flow is equal to the average flow:

$$Q_{y^*} = \bar{Q} \equiv \frac{V_{exit}(y_{end}) - V_{exit}(y_{start})}{y_{end} - y_{start}} = V'_{exit}(y^*) \tag{15}$$

where Q is the instantaneous flow ($\frac{L}{s}$), $\bar{Q}$ the average flow, y_{start} the exit tank water height at the start of the measurement and y_{end} the exit tank water height at the end of the measurement.

Now, we can determine the height y^* by inverting the relation, and subsequently find the loss coefficient:

$$y^* = (V'_{exit})^{-1} \left(\frac{V_{exit}(y_{end}) - V_{exit}(y_{start})}{y_{end} - y_{start}} \right) \tag{16}$$

$$K_v = 2g \frac{z_1 - y^*}{\bar{u}^2} \tag{17}$$

2.3 Pump Efficiency

In a pumping test, the efficiency of the check valves can be evaluated according to the ratio of input and output energy. The input energy of a piston pump can be calculated by the standard equation for work:

$$W_{in} = \int_0^T F \cdot v dt \tag{18}$$

where T is the forcing period, F is the (vertical) force on the pump piston, and v is the piston speed. The output energy of the pump system can be determined by measuring the volume flux:

$$W_{out} = p \cdot Q \tag{19}$$

where p is the outlet pressure and Q is the flow rate.

The overall efficiency coefficient therefore simply equals

$$\eta = \frac{W_{in}}{W_{out}} \tag{20}$$

3 Methods

Fluid simulations and experiments were performed to assess the performance of the check valve designs in steady state flow. In the iterative approach, advanced fluid-structure interactive simulations were time-expensive, and only a qualitative turbulence visualization was carried out.

As an exercise, and for calibrating the system, loss coefficients of a manually operated cone valve were determined and compared with literature before proceeding.

In the conclusive pump efficiency test, the original design (hinged) and selected final double-door design were used for comparison. See Fig. 10 for the full list of design versions and performed experiments.

			Simulation	Experiment	
			Flow	Flow	Pump
Design	Cone	Original		x	
	Hinged	Original	x	x	x
		Widened	x	x	
	Double door	Non-Sealed	x	x	
		Sealed	x	x	x

Figure 10: Table of experiments for each design

3.1 Simulation

3.1.1 Steady state flow simulation

The CAD software *SolidWorks* is able to simulate and analyse a crude steady state flow, directly from the modeled geometries for the check valve design. As it is a time-inexpensive, but qualitative simulation, it was performed for every model to assess its bottlenecks and the generation of turbulent vortices in the direction of the check valve flow. The inlet pressure was set equal to the expected inlet pressure in the experiment (see Sec. 3.2.1) and from the table of predicted valve loss coefficients, the outlet pressure was determined.

$$p_2 = p_1 - \Delta p \tag{21}$$

$$\Delta p = K_v \rho \frac{\bar{u}^2}{2} \tag{22}$$

3.2 Experiment

3.2.1 Steady state flow experiment

For the measurement of the check valve head loss coefficients, a setup was built to create a constant flow through an interchangeable section of piping with the check valve. With pipe losses much smaller than component losses such as bends, or mainly the check valve, relatively long sections of piping were used. This created the advantage of letting the internal flow develop as desired for the use of the loss coefficients from the literature, and made the check valve the bottleneck of the system.

Applying the Bernoulli equation (Eq. 1) to a linear piping system, in which the inlet is a constant head tank and the outlet an exit pipe, the inlet and outlet mean velocities are equal, resulting in a simplified equation:

$$z_1 = z_2 + h_L \tag{23}$$

Substituting the head loss coefficients of the other components in the system (inlets, bends, pipes), we arrive at an equation for the check valve head loss:

$$K_v = 2g\frac{z_1 - y^*}{\bar{u}^2} - K_{in} - 2K_b - K_p - K_{exit} \tag{24}$$

in which z_1 is the water height at the constant head tank, $y*$ the height of the exit tank when the instantaneous flow equals the average flow (see Sec. 2.2), $\bar{u}$ the mean outlet (and system) flow velocity, and the various loss coefficients are as described in Sec. 2.1. The initial experimental setup is shown in Fig. 12 for reference.

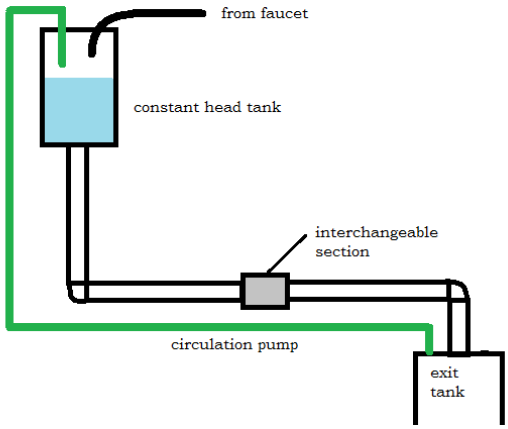

Figure 12: Photo and schematic of the initial experimental setup

It was found that the components that were expected to have the lowest loss coefficients (such as the cone valve, and the newer door valve designs) created a flux that our faucet was not able to create. Therefore we first introduced a circulation pump into the system, of which the flux was determined. This did this recreate the head tank balance, and kept the exit tank from filling too rapidly (I would like to call this "added dynamic volume capacity"), saving water in the process.

However, in this setup, occasionally air was introduced into the system. For the final experiment, a siphoning setup was introduced, to obtain water from the neighboring wave tank (See Fig. 14) without the possibility of air to get trapped inside. The circulation pump was used after each experimental run to drain the exit tank water into the wave tank again.

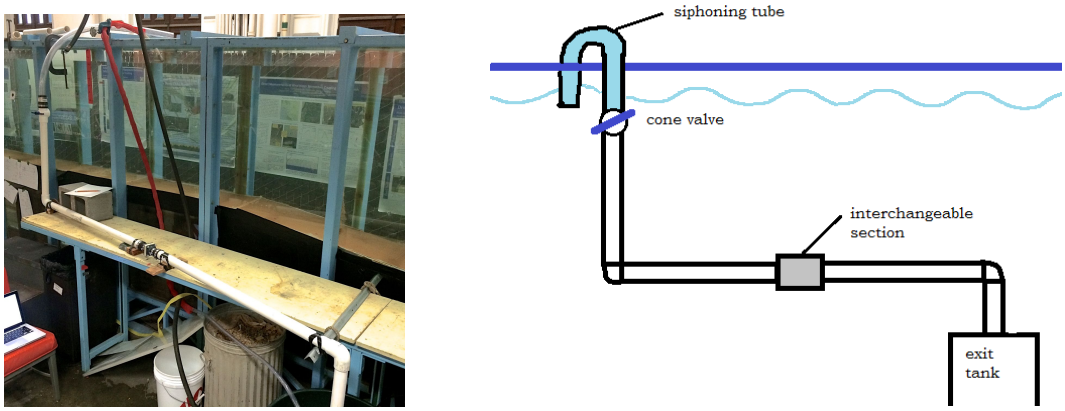

Figure 14: Photo and schematic of the second and final experimental setup

3.2.2 Pump Efficiency Test

The *TAFLab*'s existing pump efficiency tester was created by a rotating DC motor, connected via a force sensor to the pump piston (See Fig. 15). The stroke length and frequency were determined by a webcam providing live feedback about the amplitude and speed of the piston (using a Fourier fit), and the force measurements were logged using *LABView*. From this data, the input energy was calculated. The output energy was found by measuring the flow after an interchangeable vertical section of piping, so that a certain outlet pressure could be tested.

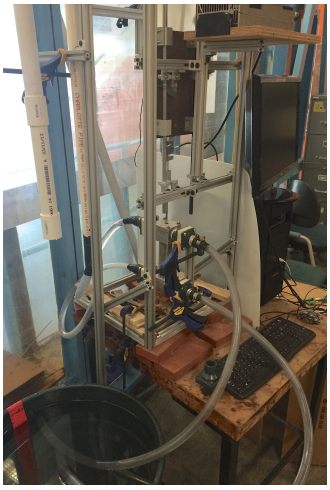

Figure 15: Pump testing setup

4 Design

4.1 Original Hinged Check Valve

The hinge check valve originally used in the wave carpet prototype, had two main design features restricting the flow in the open position of the valve - constricting orifices and a hinge that did not completely fold away.

4.1.1 Constricting Orifices

Upon first inspection, the sealing capabilities of the original hinged valve were good - the rubber on the hinge created a nearly airtight seal. However, it was observed that the interior had two circular orifices constricting the flow at the in- and outlet. As the hinge is held firmly in place by protrusions and cutouts in the base parts, it was ruled out that these constrictions were in place to keep the hinge from flowing away into the pipe. A possible explanation is for pipe insertions with a smaller diameter, or for added strength. For our setup however, these pieces were only blocking the flow. A first modification step was to remove the orifices to create a "widened hinge valve". For the engineering drawings of the original valve see Appendix B.1.

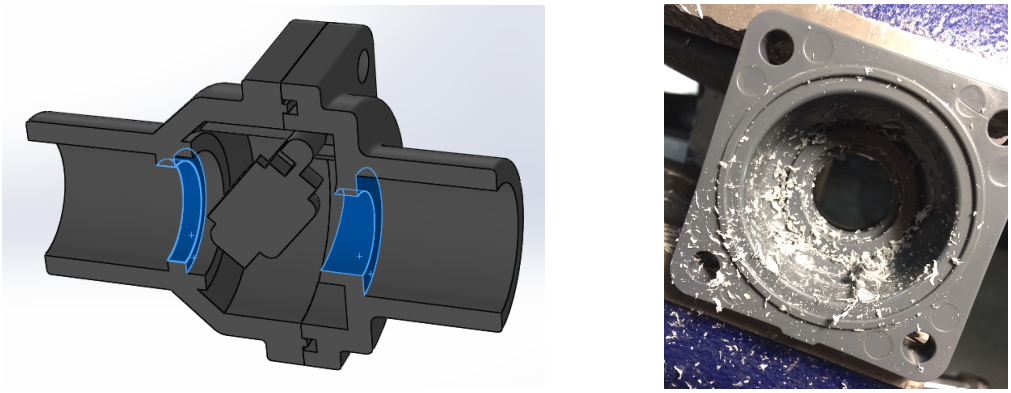

Figure 17: Identification and removal of restricting orifices

4.1.2 Opening Characteristics

When the flow is sufficient to fully open a hinge valve, it is desired that the hinge is nearly completely folded away for unobstructed flow (gravity keeps it from becoming perfectly horizontal). However, the completely opened valve still had the hinge hanging far below horizontal, blocking half of the pipe diameter. As space inside the valve chamber was limited, this was solved by opting for a completely different type of valve. For the design of a new type of valve, see Sec. 4.2.

4.2 Double Door Valve (first design)

A double door design was selected for its expected capabilities of quickly folding into a thin aerofoil-type shape, barely obstructing the flow and possibly stabilizing any internal turbulence. For seamless integration with the existing (or widened) hinge valves, a modular component was designed in *CAD* software and printed using *FDM*, to be placed in between the upper and lower base of the existing valve (see Fig. 18). For the engineering drawings of the new valve see App. B.2.

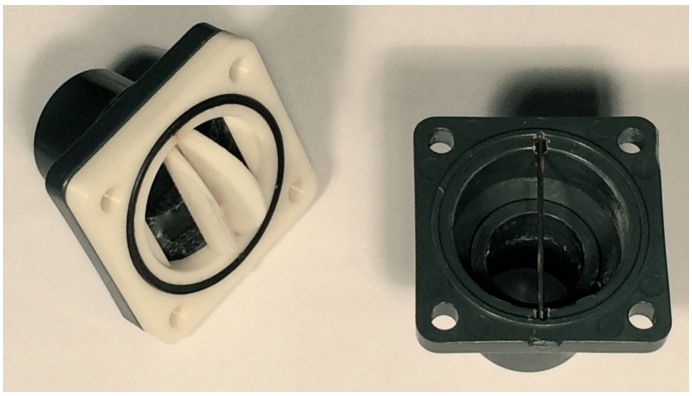

Figure 18: Design of the first door-type modular check valve component

Two identical doors are placed on a central axis, which is then put into a cutout in the modular middle base. Upon assembling the original double door design, it was observed that the doors had the possibility of both closing to one side, leaving half of the valve diameter open during the flow reversal. To prevent this from happening, a small pin was inserted behind the door axis.

4.3 Double Door Valve (second design)

Another solution to the doors closing to the same side, is a vane in the direction of the flow. It was included in the second iteration of the design, further streamlining the flow while blocking the doors from opening beyond 90° (see Fig. 19).

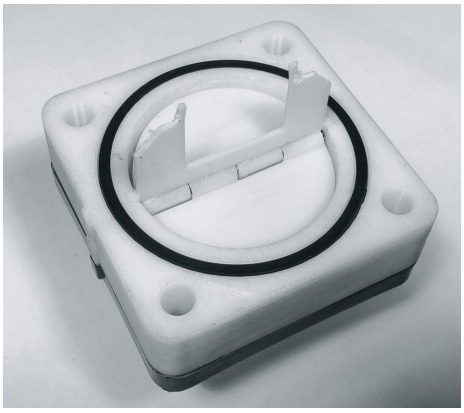

Figure 19: A vane in the direction of the flow

The sealing capabilities were improved by including an inner ledge for a precision-cut silicone seal in the shape of a Θ, sealing both at the circular edge of the doors and at the hinges (see Fig. 20). For the engineering drawings of the vanes, the seal and other new components, see App. B.3.

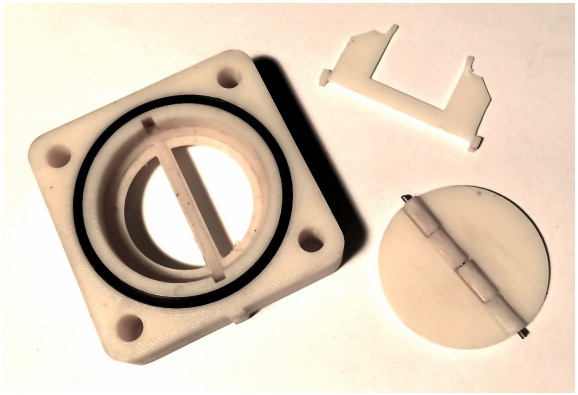

Figure 20: The $\Theta-$shaped door seal inside the assembly

5 Results

5.1 Simulation Results

5.1.1 Steady state flow simulation

In the original hinged valve design, a big variability in flow speeds was observed, for a large part because of the ring-shaped orifice constrictions (see Fig 21). Leaving the valve, it can be seen how the hinge (in a fully opened position) forces the flow through a narrow passage. Finally, we can observe turbulent vortices in the chamber, inducing more head losses.

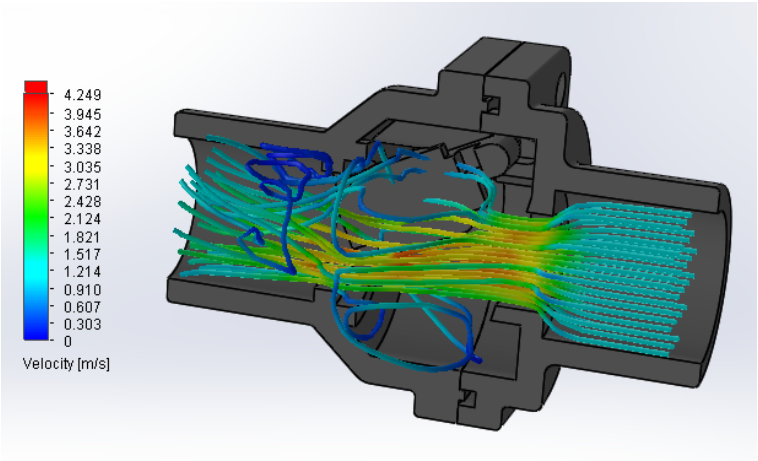

Figure 21: Steady state flow simulation for the original hinge valve

Removing the ring-shaped constrictions proved an effective way of reducing turbulences (also see the experimental results in Sec. 5.3.1). The flow speed is more constant approaching the hinge, however, there is still a narrow passageway as fluid leaves the valve.

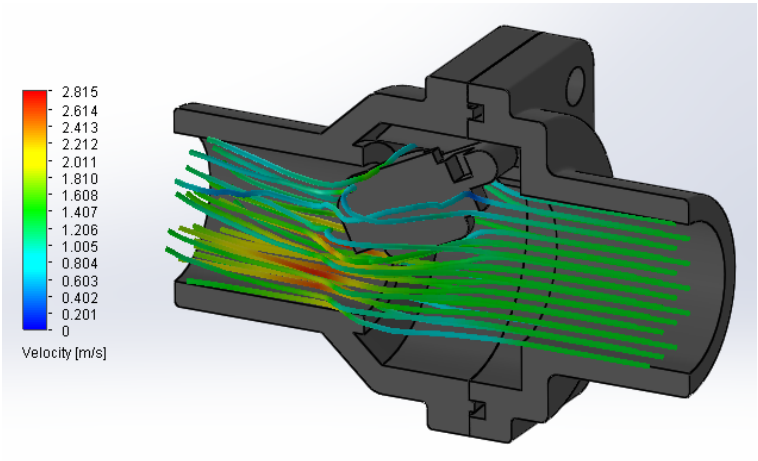

Figure 22: Steady state flow simulation for the widened hinge valve

In comparison with the hinged valves, not only do we observe much higher speeds with the double door design, also there were significantly less turbulences as the doors fold into an aerofoil-type shape (Fig. 23).

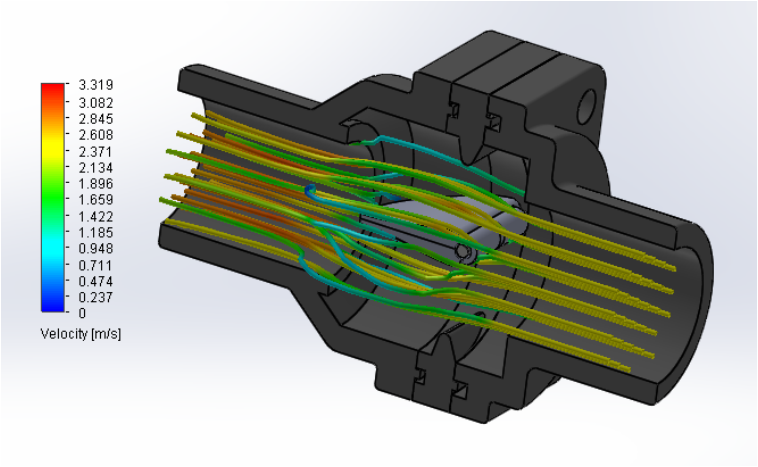

Figure 23: Steady state flow simulation for the first double door valve

The final design did not increase head losses much, as we placed an inner ring for the Θ-shaped seal and thickened the doors (Fig. 24). The flow pattern is still without major turbulences, and after experimental verification, this valve was selected as the final design, as it combined both good flowing and sealing capabilities.

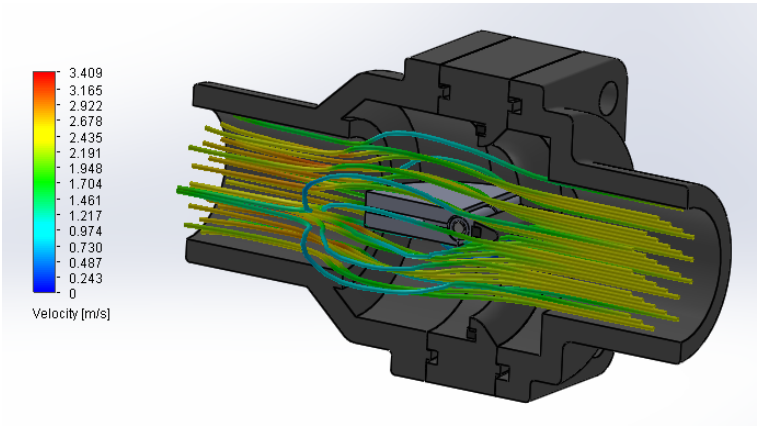

Figure 24: Steady state flow simulation for the second double door valve

5.2 Calibrations

5.2.1 Exit Tank Calibration

For accurate flux measurements, the water level in the exit tank was matched to its volume by slowly filling the tank with a measuring bucket. Water height versus added volume is displayed in Fig. 25.

Water Height (cm)	Volume (L)
0	0
5	7.7
10	15.7
15	24.5
20	32.9
25	42.0
30	50.5
35	59.2
40	68.7
45	78.3
50	84.8
55	94.9
60	105.9

Figure 25: Water height versus added volume in the exit tank

A quadratic fit was matched to the data to account for the slowly increasing diameter of the tank:

$$V_{exit} = Ah + Bh^2 \tag{25}$$

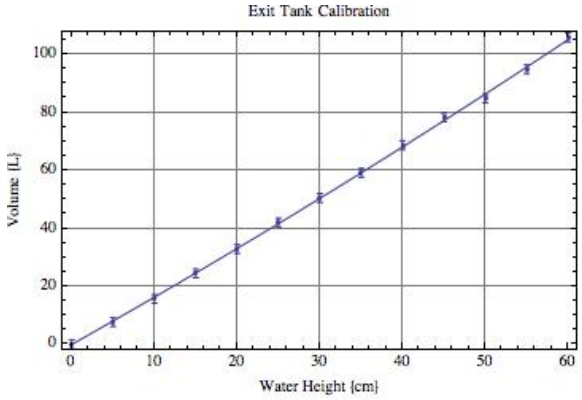

Figure 26: A quadratic fit to the exit tank volume

The best fit parameters are $A = 1.606 \pm 0.023$ L/cm and $B = 2.4 \pm 0.5 \cdot 10^{-3}$ L^2/cm.

5.2.2 Circulation Pump Calibration

The flux of the circulation pump was determined by having it empty the calibrated exit tank to the wave tank and measuring the total time. The pump itself is cylindric and has a volume of approximately 3 L, for which the volume was corrected after the water level fell below 25 cm (the pump was placed in the bottom of the tank). Time versus volume is displayed in Fig. 27.

Time (s)	Volume (L)
0.0	114.6
28.0	105.1
57.6	95.7
85.8	86.4
113.5	77.2
142.4	68.1
169.7	59.2
197.7	50.4
225.0	41.7
250.3	33.7
277.0	25.9
301.0	18.2
313.6	14.4

Figure 27: Time versus water height and tank volume for the circulation pump flux test

It was found that the pump flux is constant in time as the exit tank water level falls (see Fig. 28. It should be noted that these results are only valid for a pumping height difference comparable to our experimental setup (approx. 2m).

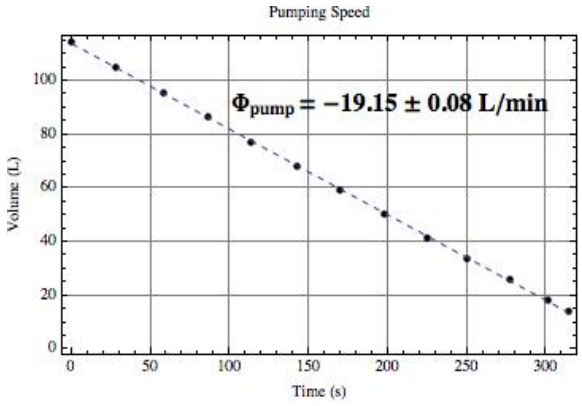

Figure 28: A linear fit for the circulation pump flux

5.2.3 System Loss Calibration

The loss coefficient of the total system was determined for a fully open cone valve, without adding any bottleneck components such as check valves. By measuring the flow, we obtain a system calibration for the subsequent experiments, since we can predict the system loss coefficient using the theory:

$$K_{pred} = K_{in} + K_{cone,open} + 2 \cdot K_{bend} + K_{pipes} + K_{exit} \tag{26}$$

The flow speed, and predicted loss coefficient are shown in Fig. 29, together with the actually measured coefficient. For the full table of results, see App. A.1.

Angle (°)	$\bar{u}$ (m/s)	K_{pred}	K_{meas}
0	1.71	4.87	10.0
0	1.66	4.89	10.5
0	1.69	4.88	10.2
0	1.68	4.89	10.3
0	1.73	4.87	9.8

Figure 29: Measurement data for the open cone valve

Now that we know the measured loss coefficient and the predicted loss coefficient of the system, we can solve for the unaccounted losses. This was taken to be the mean difference between prediction and measurement, and equals $K_{corr} = -5.28 \pm 0.22$.

5.2.4 Reproducibility of Literature Results

More cone valve measurements were taken to investigate the ability of the setup to recreate the graph of the discharge coefficients for various cone opening angles by Tullis (See. Fig 30 and 31). For the full table of results, see App. A.1. The black line is the graph for the cone valve presented in Fig. 7 by Tullis, where opening percentages have been linearly transformed to a $0 - 90°$ scale. For every experiment, a picture orthogonal to the valve was taken, and the opening angle later determined by image analysis.

Angle (°)	$\bar{u}$ (m/s)	K_v	C_d
17.3	0.22	617 ± 16	$4.02 \pm 0.05 \cdot 10^{-2}$
28.7	0.50	103 ± 3	$9.81 \pm 0.14 \cdot 10^{-2}$
47.6	1.10	13.6 ± 1.0	0.262 ± 0.009
57.8	1.32	6.2 ± 0.9	0.37 ± 0.03
67.2	1.47	2.9 ± 0.8	0.51 ± 0.06
81.6	1.64	0.5 ± 0.8	0.82 ± 0.22

Figure 30: Measurement data for the cone valve at various angles

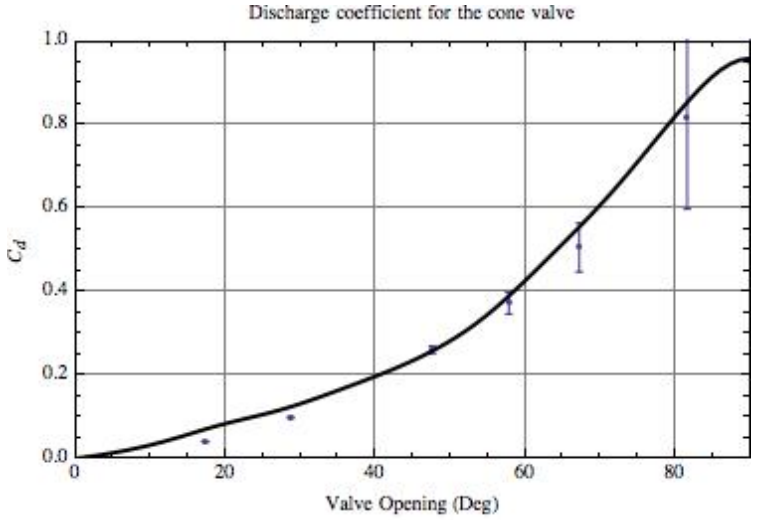

Figure 31: Measured discharge coefficients C_d of the cone valve versus Tullis' predictions

The overlap is sufficient that we assume we have validated our experiment. The line may not be over the first two points (for the smallest two angles) since it is assumed to cross the axis when the valve starts opening. For sealing purposes however, upon opening, cone valves have a couple of 'dead' degrees where the valve is still closed, so the black line could intersect the x-axis more to the right.

After this experimental validation we could proceed with analyzing the new check valve designs.

5.3 Experimental Results

5.3.1 Steady state flow experiment

With the calibrated setup we could start measuring the flow through the valves in the designed direction (D) and the reversed direction (R). The reverse flow through the original valve could not be quantified, since it sealed completely ($K_{v,R} = \infty$). See Fig. 32 for the table of results. A complete table is given in App. A.2.

Model	D/R	Test	K_v
Original Hinge	D	1	57.3 ± 1.8
		2	57.2 ± 1.6
		3	57.2 ± 1.8
Widened Hinge	D	1	46.0 ± 1.5
		2	44.9 ± 1.5
		3	47.4 ± 1.5
	R	1	$8.7 \pm 1.7 \cdot 10^4$
Door Valve V1	D	1	5.6 ± 0.8
		2	6.9 ± 0.9
		3	7.0 ± 0.9
	R	1	722 ± 21
		2	740 ± 15
		3	760 ± 30
Door Valve V2	D	1	8.4 ± 0.9
		2	7.9 ± 1.0
		3	8.7 ± 0.9
	R	1	$1.4 \pm 0.3 \cdot 10^6$

Figure 32: Measured head loss coefficients for four different valves and their sealing capabilities

It can be seen that widening the original valve had an significant effect by bringing down the loss coefficient from $K_{v,D} = 57.2 \pm 1.0$ to 46.1 ± 0.9, but slightly compromised sealing capabilities in the process ($K_{v,R} = 8.7 \pm 1.7 \cdot 10^4$). The first door design barely obstructed the flow ($K_{v,D} = 6.4 \pm 0.5$), but since no seal was included, a relatively large amount of backflow was possible ($K_{v,R} = 738 \pm 11$).

Compared to the first door design, the second version compromised a slight increase in the head losses in the flow direction ($K_{v,D} = 8.4 \pm 0.5$) with a significantly better performance in the reverse direction ($K_{v,R} = 1.4 \pm 0.3 \cdot 10^6$). Still, compared to the original valves, the head loss coefficients were 85% lower. Therefore, it was this design that was selected for the final pump test. It was expected that with higher water counterpressures from the piston pump than in the steady state flow experiment, the seals would compress even more and shut off the remaining backflow.

Although we have confirmed that door valves induce less pressure losses compared to hinge valves, it should be noted that the values found are significantly higher than the predicted loss coefficients by the literature.

5.3.2 Pump Efficiency Test

For the pump efficiency test, we replicated a setup with an outlet pipe of 1.30 ± 0.01 m high, the maximum stroke length ($L_s = 0.129 \pm 0.001$ m) and a short period (1.11s in the first and 1.49s in the second experiment). In the first experiment, the efficiency of the wave carpet pump was tested with the original valves. In the second experiment the valves were replaced by the final version of the double door valves. The results over one period (a full period is considered $t = 100$) are displayed in Fig. 34. Forces (N) have been divided by a factor of 10 and velocities (m/s) multiplied by a factor of 80 to fit on the same graph with the power input (W).

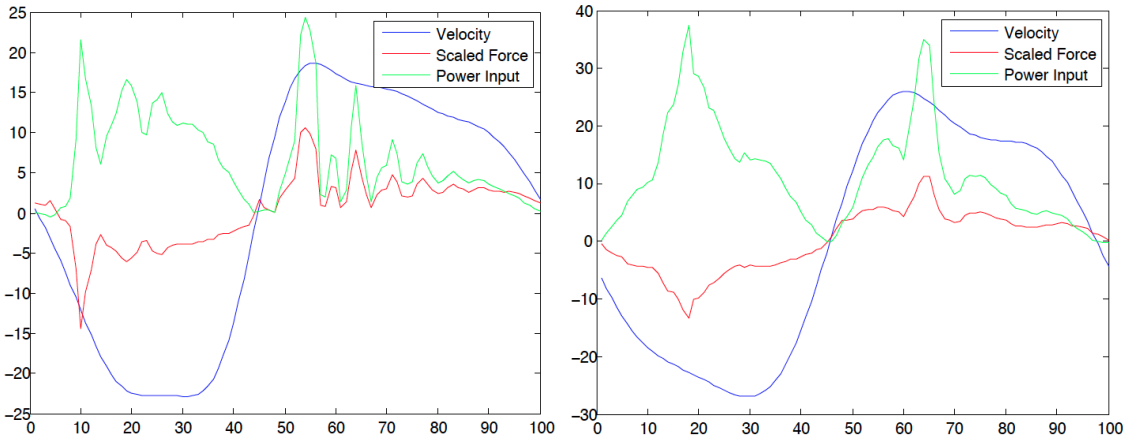

Figure 34: Pump testing results with the original hinge valve (left) and door valve (right)

In the graphs we can see that the force magnitudes remain about the same but that the profile contains less spikes for the door valve as compared to the original valve. This could indicate that there is less internal water slam, and the door valves close slower. However, slow valves induce more backflow, consequently affecting the output flux. The period in the second experiment was a little higher, and therefore the velocity and power profiles are of a slightly bigger magnitude.

The registered flux in the first experiment was $Q = 0.222 \pm 0.005$ L/s, leading to an efficiency of $41.3 \pm 0.5\%$. In the second experiment, the flux was $Q = 0.227 \pm 0.005$ L/s, leading to an efficiency of $24.7 \pm 0.5\%$.

6 Conclusion

The iterative approach in modeling and protoyping swing-type check valves has proven useful for optimizing the flow characteristics in the designed and reversed direction in a rapid evaluation cycle. An accurate measure of head losses can be obtained by the experiment described in this thesis, so that quantified decisions on the designs can be made. The head loss coefficient of the original hinge valve was brought down from $K_v = 57.2 \pm 1.0$ to 46.3 ± 1.0 in a similar design, and further down to 8.4 ± 0.4 in a double door design, without compromising much sealing capability. Steady state flow simulations were used to explore the internal fluid flow before prototyping the various designs.

The accurate prediction of the loss coefficients however remains a tough practice, as literature references are limited or only tailored to specific scenarios.

During validation of the new design in a pulsating flow in the lab's pump efficiency tester, it was shown that optimal performance in a steady state flow, both in the designed and reversed direction, does not guarantee improved results in a dynamic scenario, as the pump efficiency was decreased from $41.3 \pm 0.5\%$ to $24.7 \pm 0.5\%$. This is possibly explained by a decrease in valve speed as the doors, fully folded, do not obstruct the quickly reversing flow in the alternate direction either. A significant amount of water may flow back before the doors have the time to shut and seal.

7 Discussion and Outlook

In the short term, a safe improvement in the valve efficiencies can be made by only widening the original design through removing the constructing orifices. With a slightly bigger seal, sealing capabilities are not compromised, while improving the head losses with about 17.5%. Dynamics are expected to not be influenced much, as the hinge itself remains the same. Standards and setups for leakage testing are described in Smith's handbook [10].

In applications such as the wave carpet, dynamical behavior of the check valves is what their performance should be quantified by, rather than the steady state flow head loss coefficients. Closing speeds and the amount of backflow from the pump are examples of performance measures in a dynamical scenario. As an upscaled prototype with higher pressures is expected to be built in the near future, these characteristics should be thoroughly quantified.

Both on the simulation and experimental side, more investigation is needed. Future experimental work could include a new setup with pulsating flow, or see-through acrylic components such that the internal workings can be observed. Turbulences can be visualized by inserting particles in the flow, and the hinge/door angle in time can be recorded. On the simulation side, a fluid-structure interactive model for *CAD* components should be developed to obtain accurate numerical results directly from the digital model. In a full-scale model of the wave carpet, the separate contributions to the total efficiency can be assessed, so that it will be clear how much the valves affect the total losses.

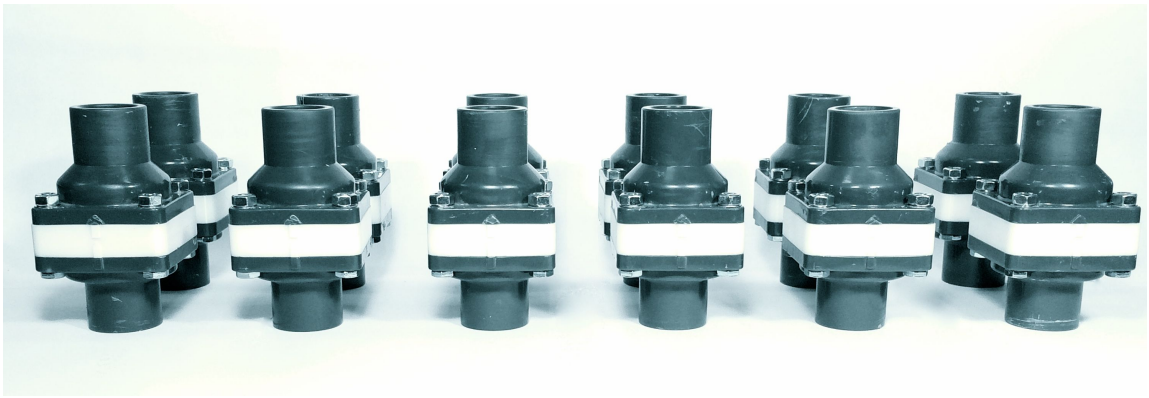

Figure 35: Twelve assemblies of the second double door valve design

References

[1] Theoretical and Applied Fluid Dynamics Laboratory, University of California, Berkeley `http://taflab.berkeley.edu/`

[2] Lehmann, M., Elandt, R., Pham, H., Ghorbani, R., Shakeri, M., and Alam, M.-R. (2013), An artificial seabed carpet for multidirectional and broadband wave energy extraction: Theory and Experiment, *Proceedings of 10th European Wave and Tidal Energy Conference (EWTEC2013)* Aalborg, Denmark

[3] Alam, M.-R. (2012), A flexible seafloor carpet for high-performance wave energy extraction, *The 31st International Conference on Ocean, Offshore and Arctic Engineering (OMAE 2012)*, Rio de Janeiro, Brazil

[4] Miller, Donald S. (1971), Internal Flow: A Guide To Losses in Pipe and Duct Systems, *The British Hydromechanics Research Association*, Cranfield, Bedford, UK

[5] Colebrook, C.F. (1939), Turbulent flow in pipes, with particular reference to the transition region between smooth and rough pipe laws, *Journal of the Institution of Civil Engineers*, London, UK

[6] Brki, D. (2011), Review of explicit approximations to the Colebrook relation for flow friction, *Journal of Petroleum Science and Engineering*, 77(1), pp34-48

[7] Tullis, J. Paul (2007), Hydraulics of Pipelines: Pumps, valves, cavitation, transients, *John Wiley & Sons, Inc.*, Hoboken, USA

[8] Jianhua, W., Wanzheng, A., and Zhou, Q. (2010), Head loss coefficient of orifice plate energy dissipator, *Journal of Hydraulic Research*, 48(4), pp526-530

[9] Benedict, Robert P. (1980), Fundamentals of Pipe Flow, *John Wiley & Sons, Inc.*, New York, USA

[10] Smith, P. and Zappe, R.W. (2004), Valve Selection Handbook: Engineering Fundamentals for Selecting the Right Valve Design for Every Industrial Flow Application, *Gulf Professional Publishing*, Burlington, USA

A Measurement Results

A.1 Calibration Measurements

Water Height (cm)	Volume (L)
0	0
5	7.7
10	15.7
15	24.5
20	32.9
25	42.0
30	50.5
35	59.2
40	68.7
45	78.3
50	84.8
55	94.9
60	105.9

Figure 36: Water height versus added volume in the exit tank

Time (s)	Water Height (cm)	Volume (L)
0.0	65	114.6
28.0	60	105.1
57.6	55	95.7
85.8	50	86.4
113.5	45	77.2
142.4	40	68.1
169.7	35	59.2
197.7	30	50.4
225.0	25	41.7
250.3	20	33.7
277.0	15	25.9
301.0	10	18.2
313.6	7.5	14.4

Figure 37: Time versus water height and tank volume for the circulation pump flux test

$L = 5.16 \pm 0.02\text{m}$
$R = 0.0389 \pm 0.0005\text{m}$
$D = 0.04075 \pm 0.0001\text{m}$
$k = 1.50 \pm 0.01 \cdot 10^{-6}$
$g = 9.81\text{m/s}^2$
$K_{in} = 0.5$
$K_{exit} = 1$

Angle (°)	z_1 (m)	h_{start}	h_{stop}	$y^*(m)$	$\bar{u}$ (m/s)	Time (s)	R_e	α_{R_e}	K_{pred}	K_{meas}
0	1.00	-0.65	-0.35	-0.50	1.71	22.53	$7.8 \cdot 10^4$	1.3	4.87	10.0
0	1.00	-0.60	-0.35	-0.48	1.66	19.22	$7.6 \cdot 10^4$	1.3	4.89	10.5
0	1.00	-0.625	-0.325	-0.48	1.69	22.88	$7.7 \cdot 10^4$	1.3	4.88	10.2
0	1.00	-0.625	-0.325	-0.48	1.68	23.03	$7.7 \cdot 10^4$	1.3	4.89	10.3
0	1.00	-0.675	-0.325	-0.50	1.73	26.3	$7.9 \cdot 10^4$	1.3	4.87	9.8

Figure 38: Measurement data for the open cone valve (uncalibrated)

Angle (°)	z_1 (m)	h_{start}	h_{stop}	$y^*(m)$	$\bar{u}$ (m/s)	Time (s)	R_e	α_{R_e}	K_v	C_d
17.3	1.00	-0.675	-0.50	-0.59	0.22	99.43	$1.0 \cdot 10^4$	2.2	617 ± 16	$4.02 \pm 0.05 \cdot 10^{-2}$
28.7	1.00	-0.60	-0.50	-0.48	0.50	63.43	$2.3 \cdot 10^4$	2.0	103 ± 3	$9.81 \pm 0.14 \cdot 10^{-2}$
47.6	1.00	-0.65	-0.35	-0.50	1.10	35.12	$5.0 \cdot 10^4$	1.8	13.6 ± 1.0	0.262 ± 0.009
57.8	1.00	-0.625	-0.35	-0.49	1.32	26.65	$6.1 \cdot 10^4$	1.6	6.2 ± 0.9	0.37 ± 0.03
67.2	1.00	-0.575	-0.525	-0.45	1.47	21.71	$6.7 \cdot 10^4$	1.3	2.9 ± 0.8	0.51 ± 0.06
81.6	1.00	-0.575	-0.525	-0.45	1.64	19.54	$7.5 \cdot 10^4$	1.3	0.5 ± 0.8	0.82 ± 0.22

Figure 39: Measurement data for the cone valve at various angles (calibrated)

A.2 Valve Measurements

Model	D/R	Test	z_1 (m)	h_{start}	h_{stop}	$y^*(m)$	$\bar{u}$ (m/s)	Time (s)	R_e	α_{R_e}	K_b	K_{pipe}	K_v
Original Hinge	D	1	1.07	-0.675	-0.40	-0.54	0.68	51.90	$3.1 \cdot 10^4$	1.66	0.55	2.96	57.5 ± 1.8
		2	1.07	-0.70	-0.35	-0.53	0.68	66.97	$3.1 \cdot 10^4$	1.66	0.55	2.96	57.3 ± 1.6
		3	1.07	-0.675	-0.40	-0.54	0.68	51.86	$3.1 \cdot 10^4$	1.66	0.55	2.96	57.4 ± 1.8
Widened Hinge	D	1	1.07	-0.70	-0.40	-0.55	0.74	51.65	$3.4 \cdot 10^4$	1.60	0.53	2.90	46.1 ± 1.5
		2	1.07	-0.70	-0.40	-0.55	0.76	51.15	$3.5 \cdot 10^4$	1.60	0.53	2.89	45.0 ± 1.5
		3	1.07	-0.675	-0.35	-0.51	0.73	57.53	$3.3 \cdot 10^4$	1.60	0.53	2.91	47.6 ± 1.5
	R†	1	1.00			0.06	0.0147	161.0	$6.7 \cdot 10^2$	2.20	0.73	12.2	$8.7 \pm 1.7 \cdot 10^4$
Door Valve V1	D	1	1.07	-0.75	-0.40	-0.58	1.42	31.87	$6.5 \cdot 10^4$	1.40	0.46	2.51	5.6 ± 0.8
		2	1.07	-0.675	-0.35	-0.51	1.34	31.31	$6.1 \cdot 10^4$	1.40	0.46	2.55	7.0 ± 0.9
		3	1.07	-0.675	-0.35	-0.51	1.34	31.36	$6.1 \cdot 10^4$	1.40	0.46	2.55	7.0 ± 0.9
	R	1	1.07	-0.65	-0.50	0.06	0.16	115.0	$7.5 \cdot 10^3$	1.40	0.46	4.22	722 ± 21
		2	0.87	-0.65	-0.35	0.06	0.15	265.7	$6.7 \cdot 10^3$	1.40	0.46	4.37	740 ± 15
		3	0.87	-0.55	-0.45	0.06	0.14	86.99	$6.6 \cdot 10^3$	1.40	0.46	4.39	760 ± 30
Door Valve V2	D	1	1.07	-0.70	-0.35	-0.53	1.29	35.12	$5.9 \cdot 10^4$	1.40	0.46	2.57	8.4 ± 0.9
		2	1.07	-0.675	-0.425	-0.55	1.32	24.23	$6.0 \cdot 10^4$	1.40	0.46	2.56	8.0 ± 1.0
		3	1.07	-0.65	-0.35	-0.50	1.27	30.37	$5.8 \cdot 10^4$	1.40	0.46	2.58	8.7 ± 0.9
	R†	1	1.00			0.06	0.0036	643.2	$1.6 \cdot 10^2$	2.20	0.73	48.6	$1.4 \pm 0.3 \cdot 10^6$

Figure 40: Measured head loss coefficients for four different valves and their sealing capabilities

†Output flux was not measured here with the exit tank due to the low flow speeds. A measuring glass was used instead.

B Engineering Drawings

B.1 Original Hinged Valve

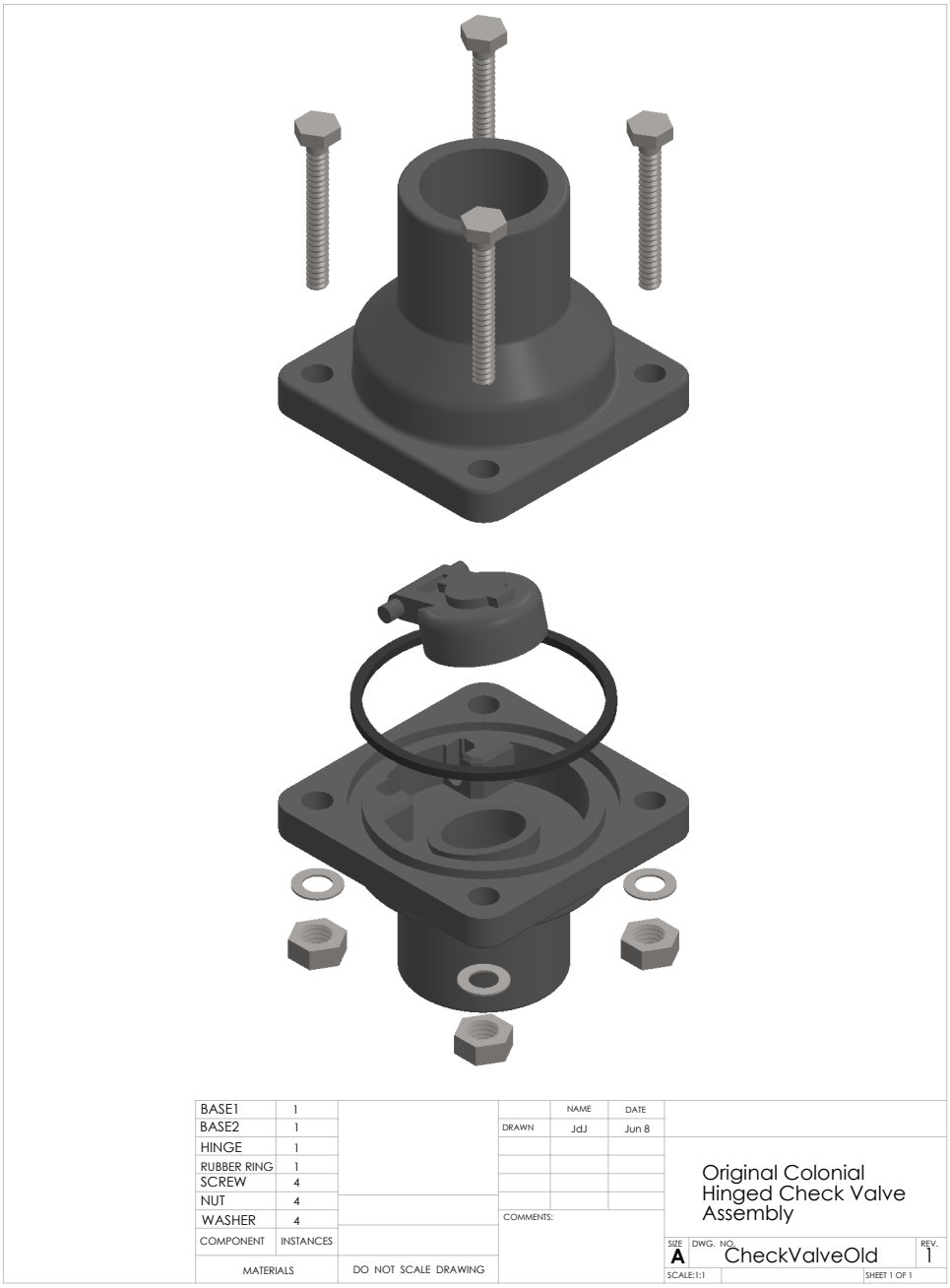

BASE1	1			NAME	DATE
BASE2	1		DRAWN	JdJ	Jun 8
HINGE	1				
RUBBER RING	1				
SCREW	4				
NUT	4		COMMENTS:		
WASHER	4				
COMPONENT	INSTANCES				
MATERIALS		DO NOT SCALE DRAWING			

Original Colonial Hinged Check Valve Assembly

SIZE	DWG. NO.	REV.
A	CheckValveOld	1
SCALE:1:1		SHEET 1 OF 1

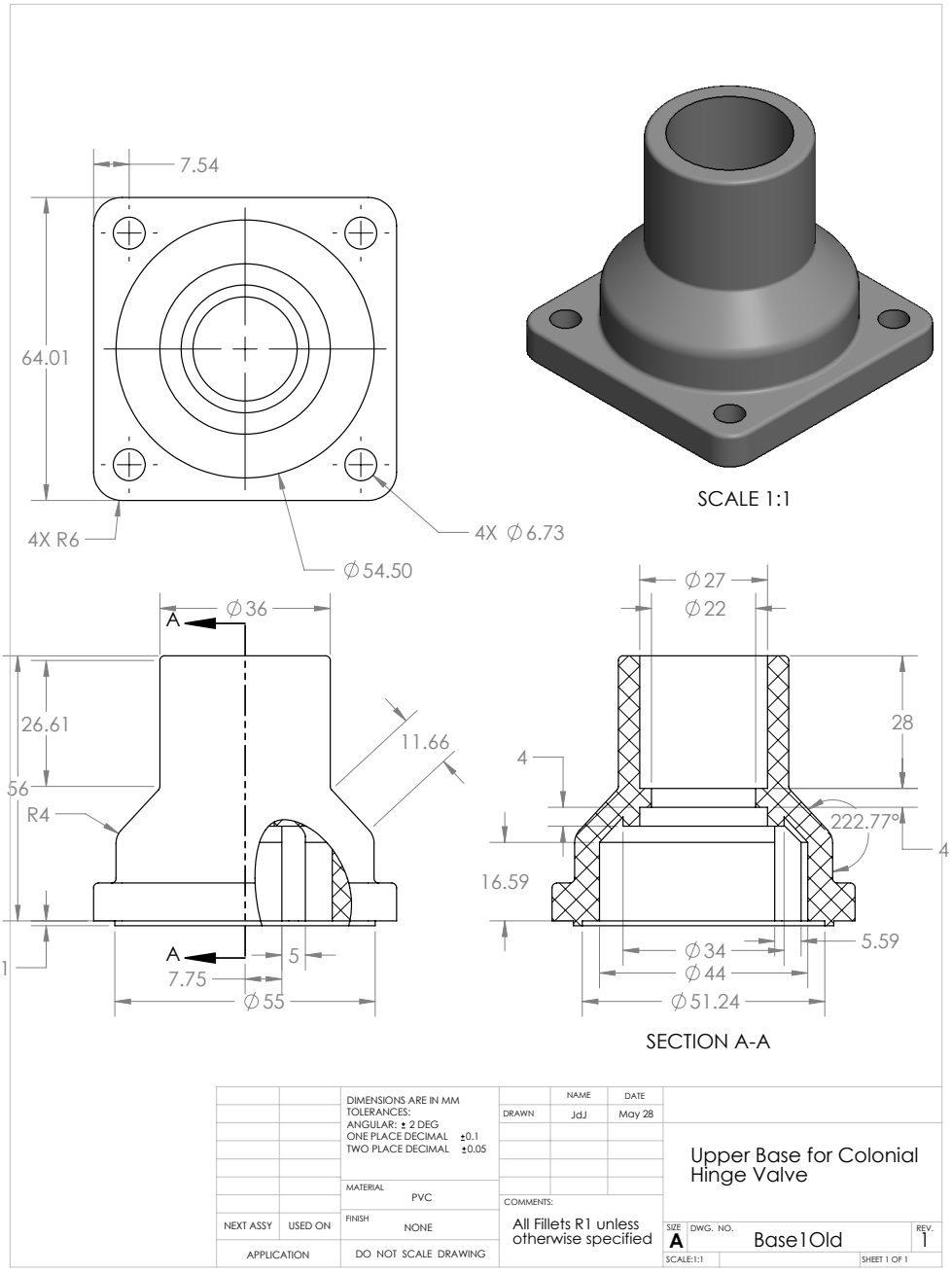
7.54
64.01
4X R6
4X ∅6.73
∅54.50
SCALE 1:1
∅36
A
26.61
56
R4
11.66
1
A
5
7.75
∅55
∅27
∅22
28
4
222.77°
4
16.59
5.59
∅34
∅44
∅51.24
SECTION A-A
DIMENSIONS ARE IN MM
TOLERANCES:
ANGULAR: ± 2 DEG
ONE PLACE DECIMAL ±0.1
TWO PLACE DECIMAL ±0.05
MATERIAL
PVC
FINISH
NONE
NEXT ASSY
USED ON
APPLICATION
DO NOT SCALE DRAWING
NAME
DATE
DRAWN
JdJ
May 28
COMMENTS:
All Fillets R1 unless otherwise specified
Upper Base for Colonial Hinge Valve
SIZE
A
DWG. NO.
Base1Old
REV.
1
SCALE:1:1
SHEET 1 OF 1

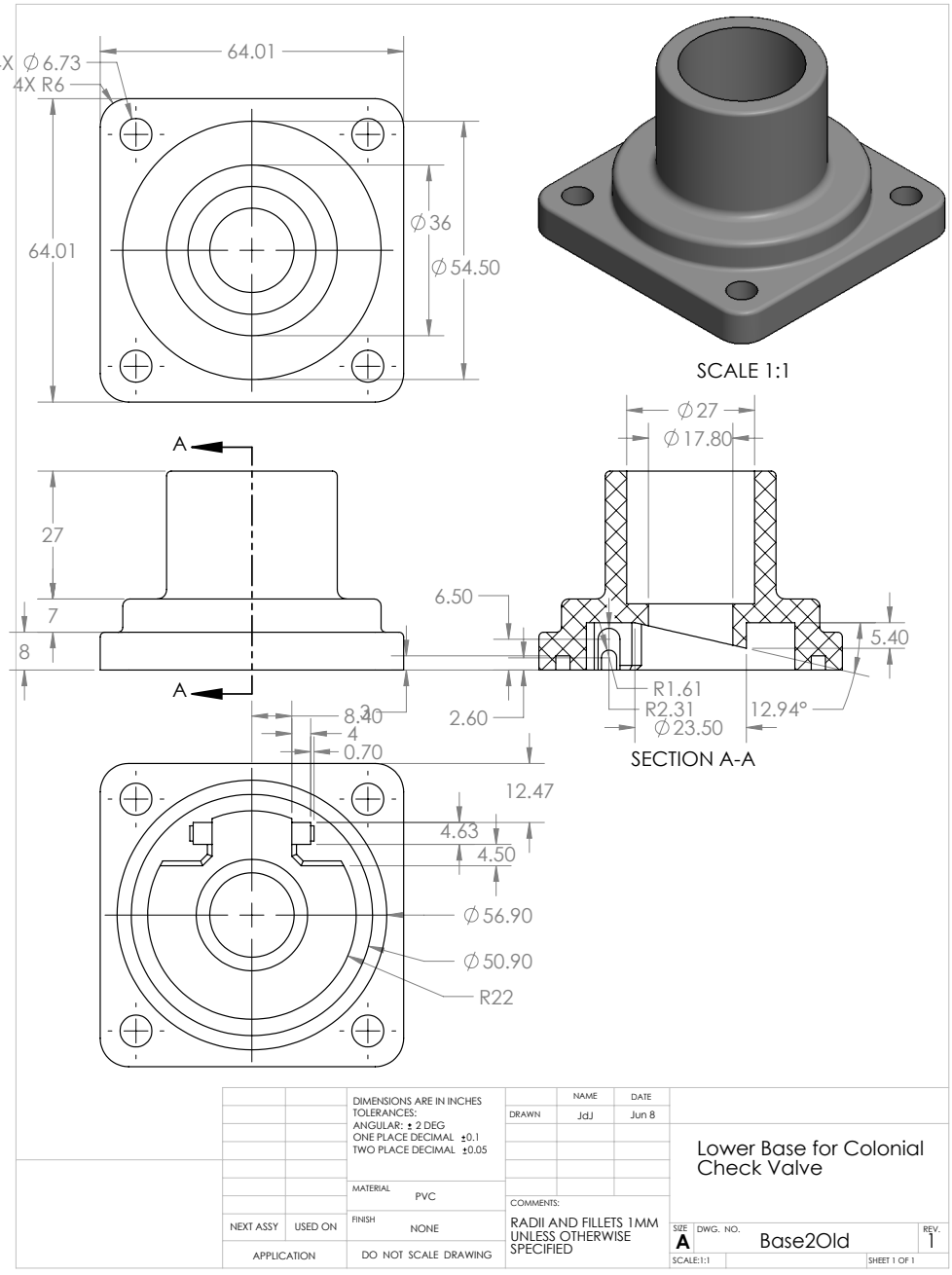

		DIMENSIONS ARE IN INCHES TOLERANCES: ANGULAR: ± 2 DEG ONE PLACE DECIMAL ±0.1 TWO PLACE DECIMAL ±0.05		NAME	DATE
			DRAWN	JdJ	Jun 8
		MATERIAL PVC	COMMENTS:		
NEXT ASSY	USED ON	FINISH NONE	RADII AND FILLETS 1MM UNLESS OTHERWISE SPECIFIED		
APPLICATION		DO NOT SCALE DRAWING			

Lower Base for Colonial Check Valve

SIZE	DWG. NO.	REV.
A	Base2Old	1
SCALE:1:1		SHEET 1 OF 1

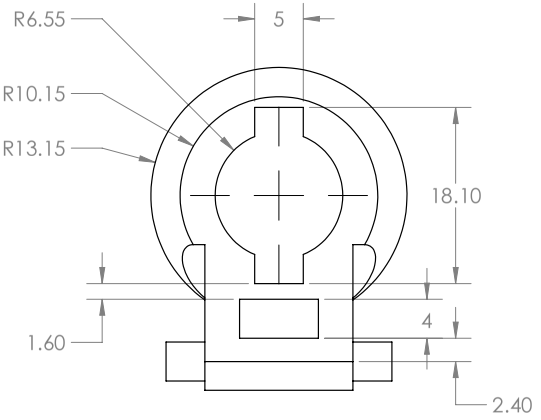

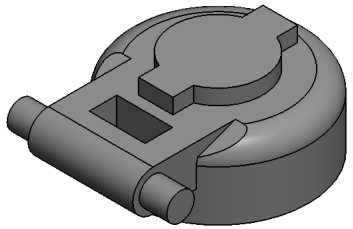

SCALE 2:1

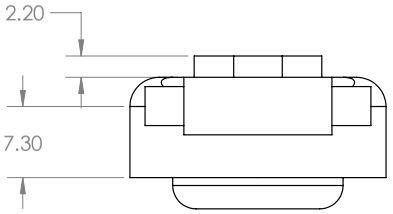

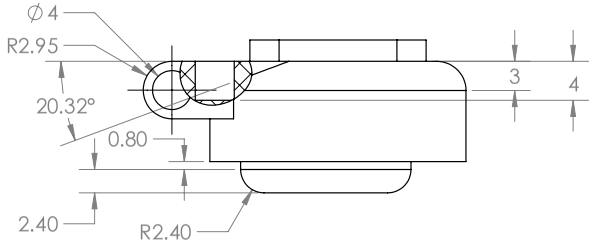

		UNLESS OTHERWISE SPECIFIED:		NAME	DATE
		DIMENSIONS ARE IN MM TOLERANCES: ANGULAR: ± 2 DEG TWO PLACE DECIMAL ±0.05	DRAWN	JdJ	May 28
			COMMENTS:		
		MATERIAL PVC			
NEXT ASSY	USED ON	FINISH none			
APPLICATION		DO NOT SCALE DRAWING			

TITLE: Hinge Design for Colonial Check Valve

SIZE	DWG. NO.	REV
A	Hinge	1

SCALE: 2:1 SHEET 1 OF 1

5 4 3 2 1

B.2 Double Door Valve (first design)

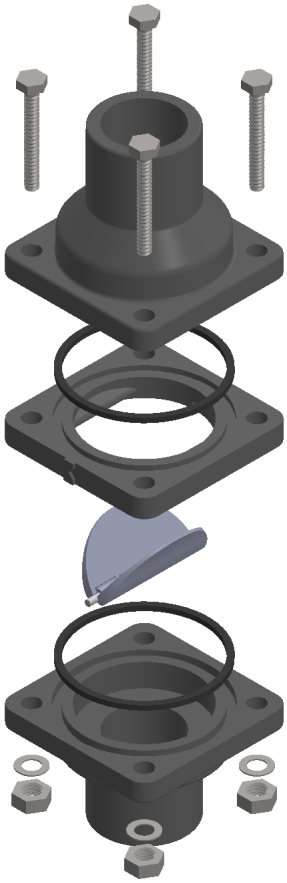

BASE1n	1	NUT	4		NAME	DATE
BASE2n	1	WASHER	4	DRAWN	JdJ	Jun 8
BASEMID	1					
RUBBER RING	2					
DOOR	2					
SPOKE	1					
SCREW	4			COMMENTS:		
COMPONENT	INSTANCES	COMPONENT	INSTANCES			
MATERIALS				DO NOT SCALE DRAWING		

Double Door Check Valve Assembly (First Design)

SIZE	DWG. NO.	REV.
A	CheckValveDoor	1
SCALE:1:1		SHEET 1 OF 1

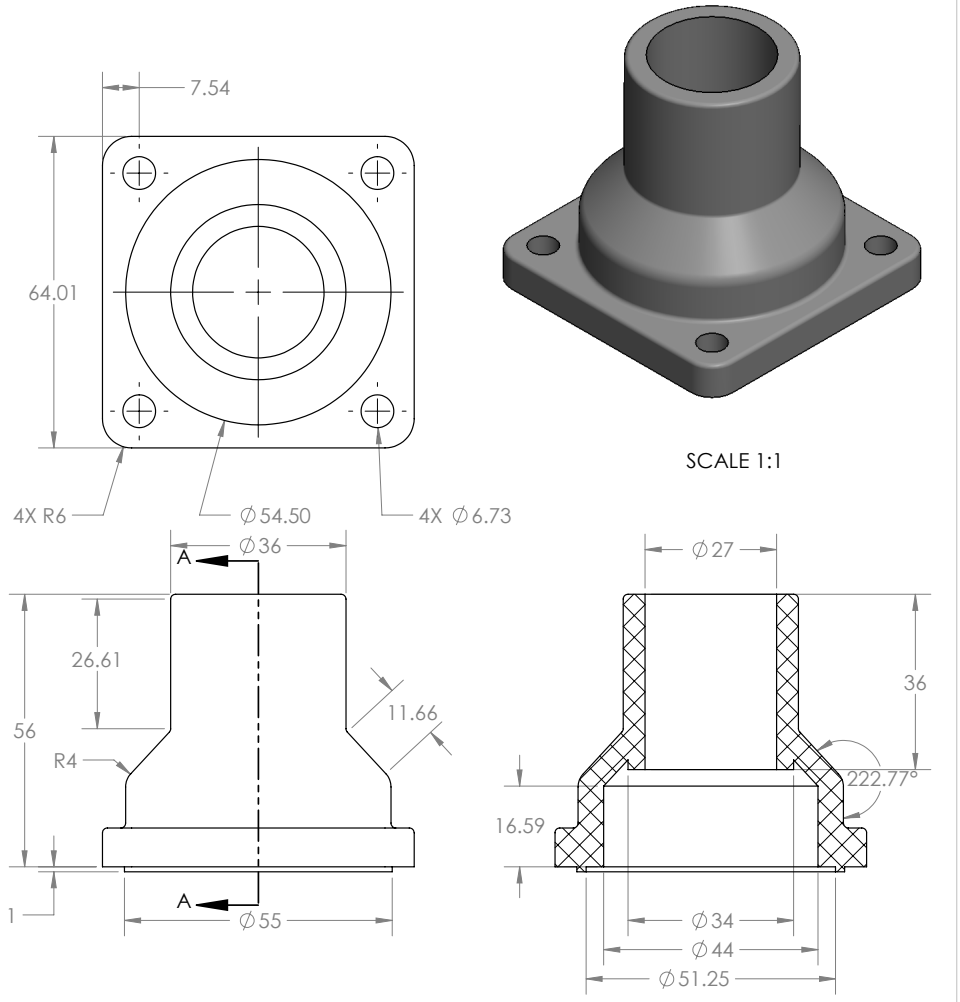

		DIMENSIONS ARE IN MM TOLERANCES: ANGULAR: ± 2 DEG ONE PLACE DECIMAL ±0.1 TWO PLACE DECIMAL ±0.05		NAME	DATE
			DRAWN	JdJ	Jun 8
		MATERIAL PVC	COMMENTS:		
NEXT ASSY	USED ON	FINISH NONE	All Fillets R1 unless otherwise specified		
APPLICATION		DO NOT SCALE DRAWING			

Upper Base for Colonial Hinge Valve (modified)

SIZE	DWG. NO.	REV.
A	Base1New	2
SCALE:1:1		SHEET 1 OF 1

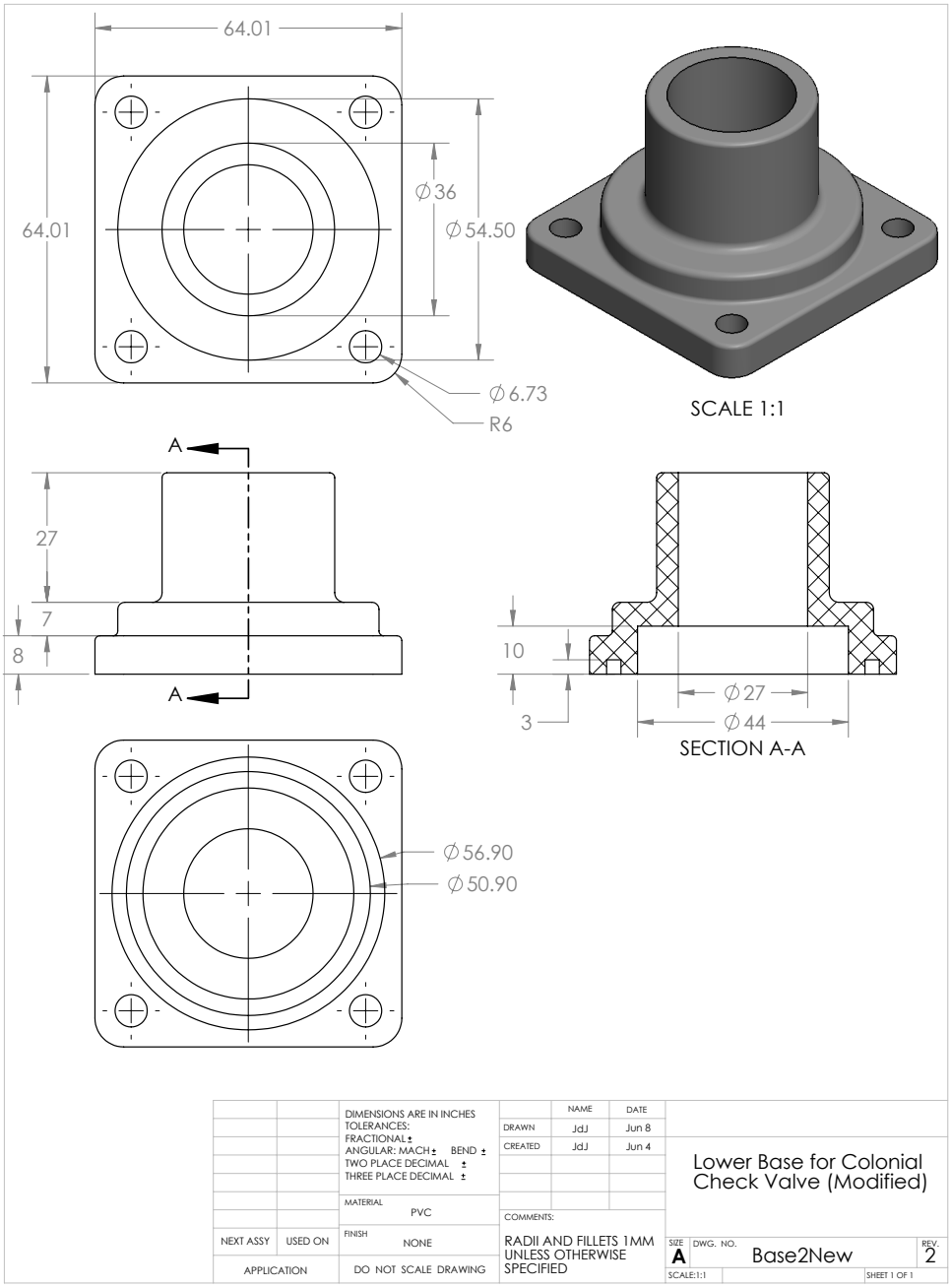

		DIMENSIONS ARE IN INCHES TOLERANCES: FRACTIONAL ± ANGULAR: MACH ± BEND ± TWO PLACE DECIMAL ± THREE PLACE DECIMAL ±		NAME	DATE
			DRAWN	JdJ	Jun 8
			CREATED	JdJ	Jun 4
		MATERIAL PVC	COMMENTS:		
NEXT ASSY	USED ON	FINISH NONE	RADII AND FILLETS 1MM UNLESS OTHERWISE SPECIFIED		
APPLICATION		DO NOT SCALE DRAWING			

Lower Base for Colonial Check Valve (Modified)

SIZE	DWG. NO.	REV.
A	Base2New	2
SCALE:1:1		SHEET 1 OF 1

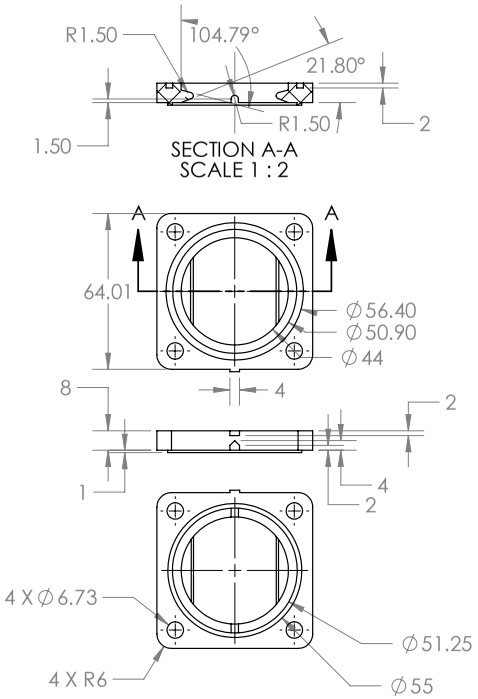

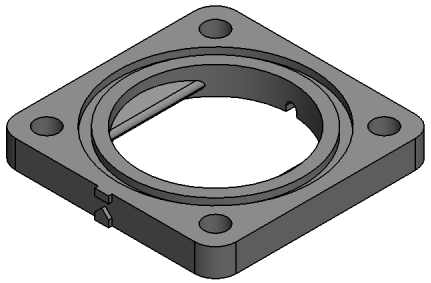

SCALE 1:1

		UNLESS OTHERWISE SPECIFIED:		NAME	DATE
		DIMENSIONS ARE IN MM TOLERANCES: ANGULAR: ± 2 DEG TWO PLACE DECIMAL ±0.05 THREE PLACE DECIMAL	DRAWN	JdJ	May 28
			PRINTED	Shop	Jun 2
			COMMENTS:		
		MATERIAL ABS+ Plastic			
NEXT ASSY	USED ON	FINISH None			
APPLICATION		DO NOT SCALE DRAWING			

TITLE:
Modular Interconnection for Colonial Hinge Valve to Double Door

SIZE	DWG. NO.	REV
A	BaseMid	1

SCALE: 1:2 | SHEET 1 OF 1

5 4 3 2 1

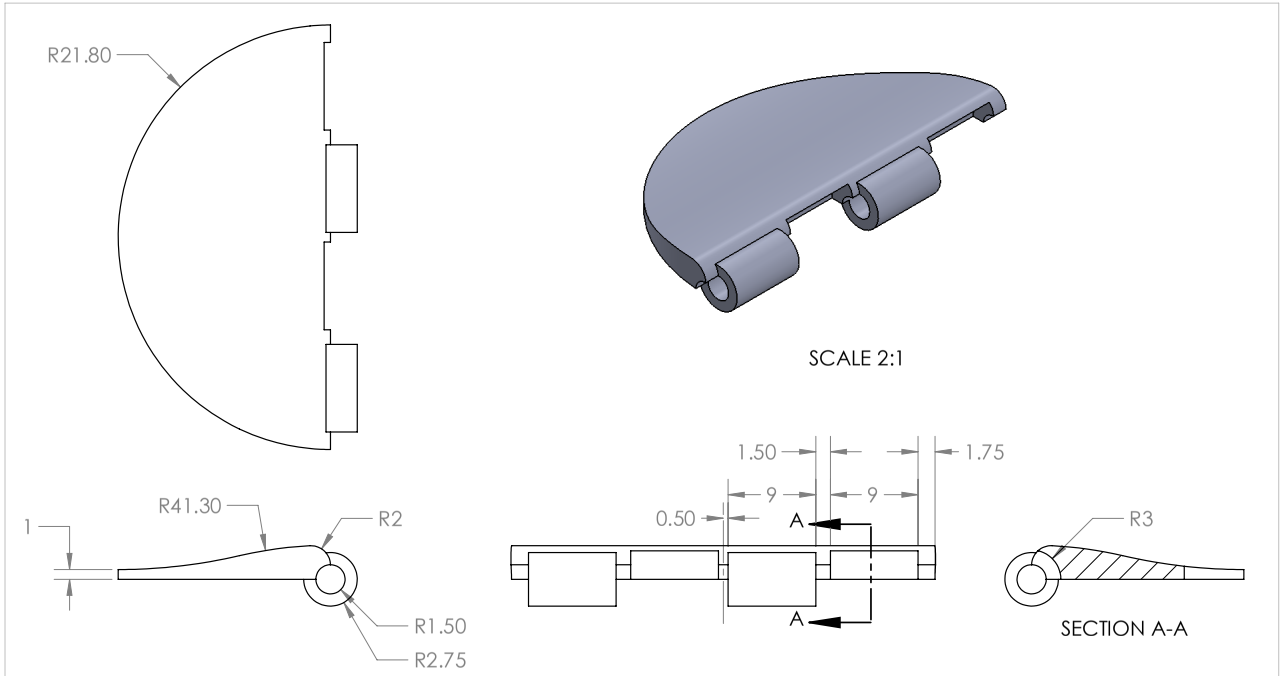

		UNLESS OTHERWISE SPECIFIED:		NAME	DATE
		DIMENSIONS ARE IN MM	DRAWN	JdJ	Jun 8
		ONE PLACE DECIMAL ±0.1 TWO PLACE DECIMAL ±0.05	PRINTED	SHOP	Jun 3
		MATERIAL ABS+ PLASTIC	COMMENTS:		
NEXT ASSY	USED ON	FINISH SANDPAPER			
APPLICATION		DO NOT SCALE DRAWING			

TITLE: Door Design

SIZE	DWG. NO.	REV
A	DoorV1	1

SCALE: 2:1 SHEET 1 OF 1

5 4 3 2 1

B.3 Double Door Valve (second design)

Upper and lower base (which are identical to previous design), not included in component drawings.

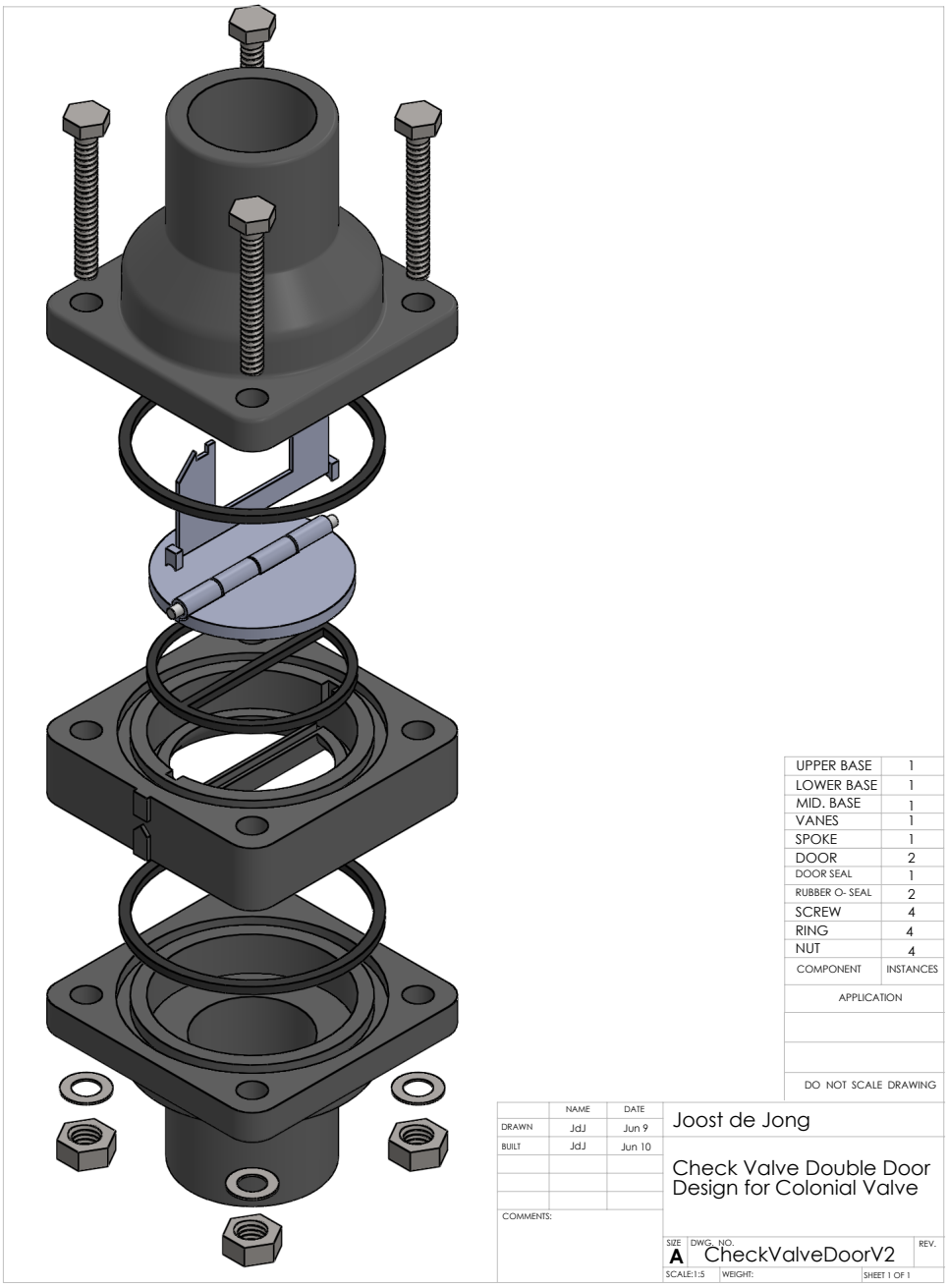

COMPONENT	INSTANCES
UPPER BASE	1
LOWER BASE	1
MID. BASE	1
VANES	1
SPOKE	1
DOOR	2
DOOR SEAL	1
RUBBER O- SEAL	2
SCREW	4
RING	4
NUT	4

APPLICATION

DO NOT SCALE DRAWING

	NAME	DATE
DRAWN	JdJ	Jun 9
BUILT	JdJ	Jun 10

COMMENTS:

Joost de Jong

Check Valve Double Door Design for Colonial Valve

SIZE A | DWG. NO. CheckValveDoorV2 | REV.

SCALE:1:5 | WEIGHT: | SHEET 1 OF 1

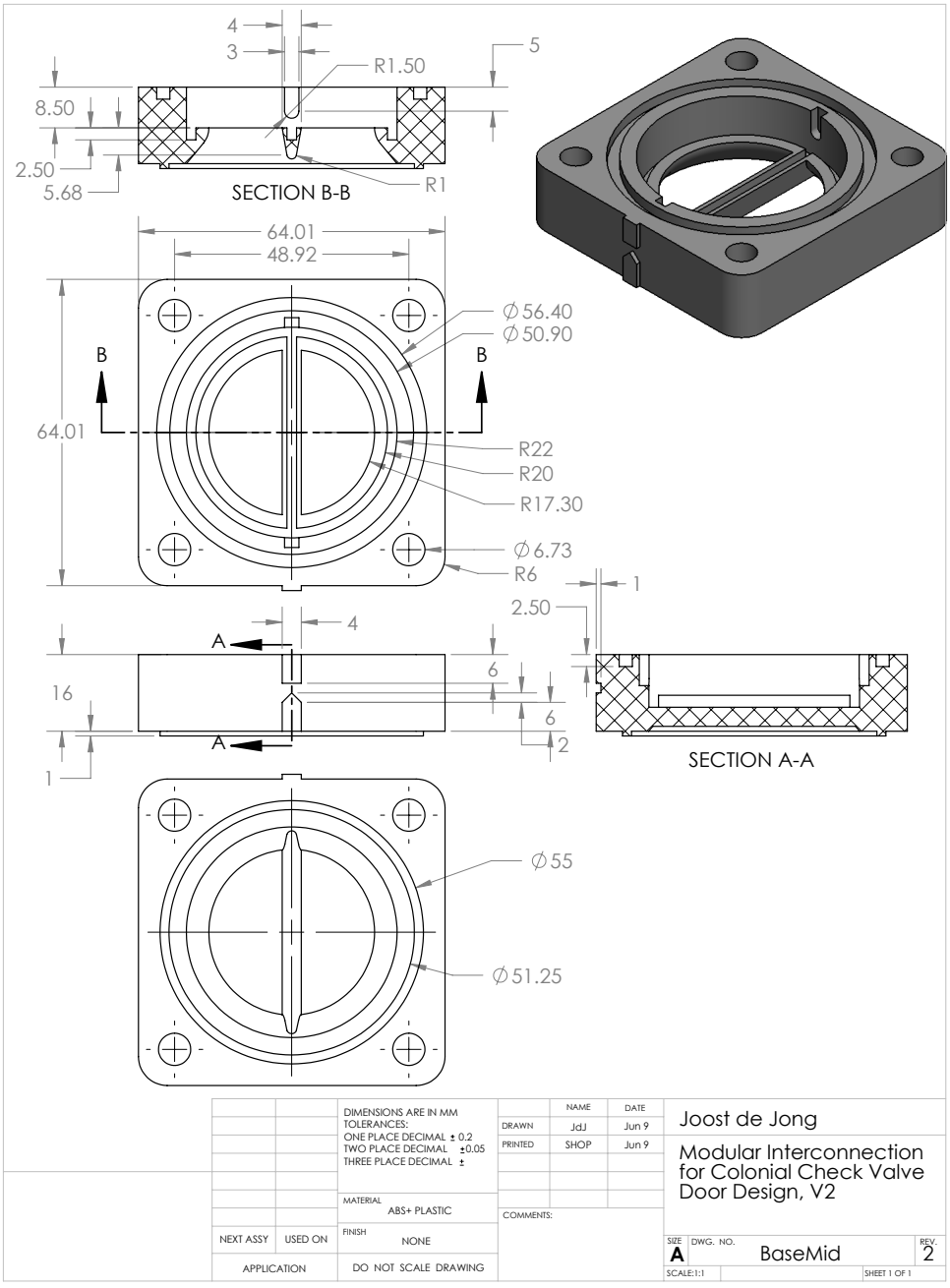
4
3
R1.50
5
8.50
2.50
5.68
R1
SECTION B-B
64.01
48.92
∅56.40
∅50.90
B
B
64.01
R22
R20
R17.30
∅6.73
R6
1
2.50
4
A
A
16
6
6
2
1
SECTION A-A
∅55
∅51.25
DIMENSIONS ARE IN MM
TOLERANCES:
ONE PLACE DECIMAL ± 0.2
TWO PLACE DECIMAL ±0.05
THREE PLACE DECIMAL ±
MATERIAL
ABS+ PLASTIC
FINISH
NONE
NEXT ASSY
USED ON
APPLICATION
DO NOT SCALE DRAWING
NAME
DATE
DRAWN
JdJ
Jun 9
PRINTED
SHOP
Jun 9
COMMENTS:
Joost de Jong
Modular Interconnection for Colonial Check Valve Door Design, V2
SIZE
A
DWG. NO.
BaseMid
REV.
2
SCALE:1:1
SHEET 1 OF 1

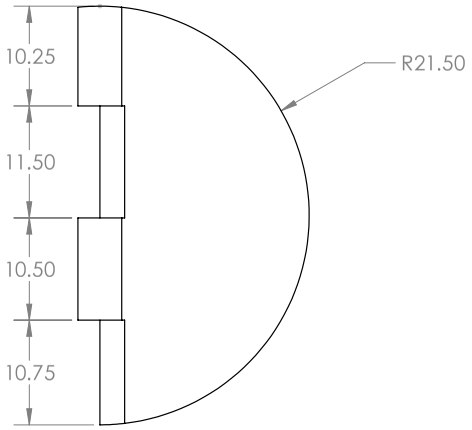

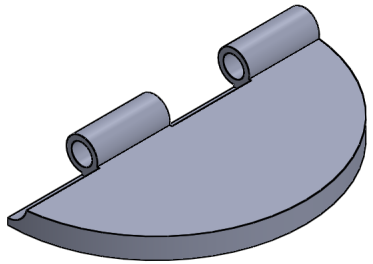

SCALE 2:1

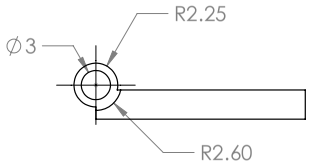

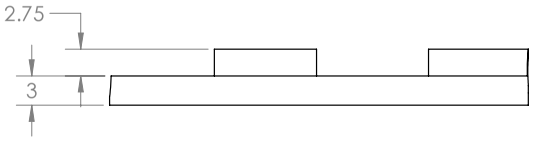

		UNLESS OTHERWISE SPECIFIED:		NAME	DATE	Joost de Jong
		DIMENSIONS ARE IN MM TOLERANCES:	DRAWN	JdJ	Jun 9	
			PRINTED	SHOP	Jun 9	TITLE:
		ONE PLACE DECIMAL ± 0.2 TWO PLACE DECIMAL ±0.05				Door Design, V2
			COMMENTS:			
		MATERIAL ABS+ PLASTIC				SIZE A / DWG. NO. Door2 / REV 2
NEXT ASSY	USED ON	FINISH NONE				
APPLICATION		DO NOT SCALE DRAWING				SCALE: 2:1 / SHEET 1 OF 1

5 4 3 2 1

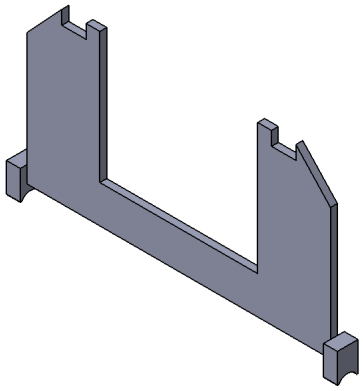

SCALE 2:1

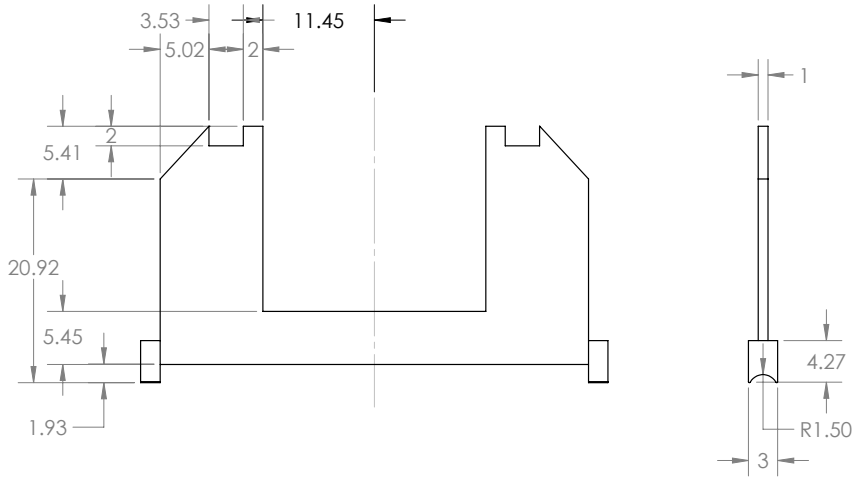

		DIMENSIONS ARE IN INCHES TOLERANCES: ONE PLACE DECIMAL ±0.1 TWO PLACE DECIMAL ±0.05		NAME	DATE
			DRAWN	JdJ	Jun 9
			PRINTED	SHOP	Jun 9
		MATERIAL ABS+ PLASTIC	COMMENTS:		
NEXT ASSY	USED ON	FINISH NONE			
APPLICATION		DO NOT SCALE DRAWING			

Joost de Jong

Stabilizing Vanes in Double Door Design V2

SIZE	DWG. NO.	REV.
A	Vanes	1
SCALE:2:1		SHEET 1 OF 1

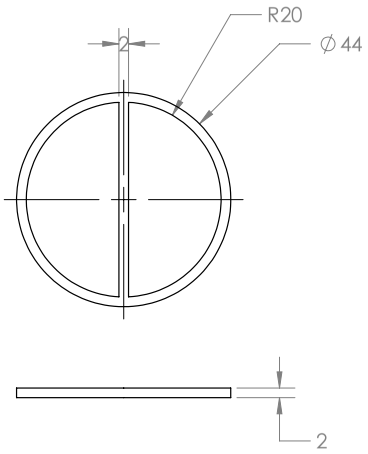

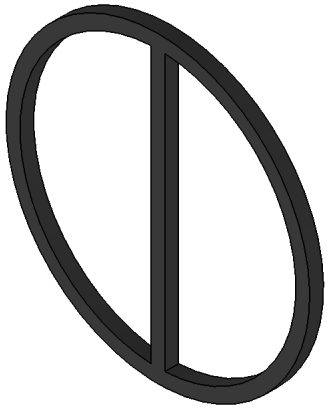

PERSPECTIVE VIEW
SCALE 2:1

		UNLESS OTHERWISE SPECIFIED:		NAME	DATE	Joost de Jong
		DIMENSIONS ARE IN MM TOLERANCES: +- 0.2mm	DRAWN	JdJ	Jun 9	TITLE:
			CUTTED	SHOP	Jun 9	Check Valve Door Seal
		MATERIAL 2MM SILICONE	COMMENTS: CUTTING PROCEDURE:			SIZE A / DWG. NO. Seal / REV 1
NEXT ASSY	USED ON	FINISH	CLAMP SILICONE SHEET BETWEEN TWO ACRYLIC PLATES FOR FIRMNESS			
APPLICATION		DO NOT SCALE DRAWING				SCALE: 1:1 / SHEET 1 OF 1

5 4 3 2 1